TWO DISTINCT SYNCHRONIZATION PROCESSES IN THE TRANSITION TO SLEEP

Two Distinct Synchronization Processes in the Transition to Sleep: A High-Density Electroencephalographic Study

Francesca Siclari, MD[1,*]; Giulio Bernardi, MD, PhD[1,2,3,*]; Brady A. Riedner, PhD[1]; Joshua J. LaRocque, BS[4]; Ruth M. Benca, MD, PhD[1]; Giulio Tononi, MD, PhD[1]

*[1]Department of Psychiatry, University of Wisconsin, Madison, Wisconsin; [2]Laboratory of Clinical Biochemistry and Molecular Biology, University of Pisa, Italy; [3]Clinical Psychology Branch, University of Pisa, AOUP Santa Chiara, Pisa, Italy; [4]Medical Scientist Training Program and Neuroscience Training Program, University of Wisconsin, Madison, Wisconsin; *co-first authors*

Objectives: To assess how the characteristics of slow waves and spindles change in the falling-asleep process.
Design: Participants undergoing overnight high-density electroencephalographic recordings were awakened at 15- to 30-min intervals. One hundred forty-one falling-asleep periods were analyzed at the scalp and source level.
Setting: Sleep laboratory.
Participants: Six healthy participants.
Interventions: Serial awakenings.
Results: The number and amplitude of slow waves followed two dissociated, intersecting courses during the transition to sleep: slow wave number increased slowly at the beginning and rapidly at the end of the falling-asleep period, whereas amplitude at first increased rapidly and then decreased linearly. Most slow waves occurring early in the transition to sleep had a large amplitude, a steep slope, involved broad regions of the cortex, predominated over frontomedial regions, and preferentially originated from the sensorimotor and the posteromedial parietal cortex. Most slow waves occurring later had a smaller amplitude and slope, involved more circumscribed parts of the cortex, and had more evenly distributed origins. Spindles were initially sparse, fast, and involved few cortical regions, then became more numerous and slower, and involved more areas.
Conclusions: Our results provide evidence for two types of slow waves, which follow dissociated temporal courses in the transition to sleep and have distinct cortical origins and distributions. We hypothesize that these two types of slow waves result from two distinct synchronization processes: (1) a "bottom-up," subcorticocortical, arousal system-dependent process that predominates in the early phase and leads to type I slow waves, and (2) a "horizontal," corticocortical synchronization process that predominates in the late phase and leads to type II slow waves. The dissociation between these two synchronization processes in time and space suggests that they may be differentially affected by experimental manipulations and sleep disorders.

Keywords: falling asleep, high-density EEG, neuronal synchronization, sleep, sleep-wake transition, slow waves, source modeling, spindles
Citation: Siclari F, Bernardi G, Riedner BA, LaRocque JJ, Benca RM, Tononi G. Two distinct synchronization processes in the transition to sleep: a high-density electroencephalographic study. *SLEEP* 2014;37(10):1621-1637.

INTRODUCTION

The transition from wakefulness to sleep is characterized by the appearance of mental imagery and behavioral unresponsiveness, changes in neuromodulation,[1] and a shift from fast-frequency, low-amplitude electroencephalographic (EEG) activity to low-frequency, high-amplitude slow waves and sleep spindles.[2,3] Despite these marked and seemingly global changes, falling asleep may actually constitute a heterogeneous process, both spatially and temporally. Recent work has shown that sleep slow oscillations and associated neural events usually do not affect the entire cortex at the same time, as was previously thought, but rather they occur locally. In particular, studies using intracerebral EEG recordings have revealed that slow waves and spindles tend to appear asynchronously across different brain regions,[3,4] and it is now established that slow waves can be regulated locally, as a function of prior use and neural plasticity.[5-8] In addition, clinical observations indicate that some sleep disorders, such as sleepwalking, reflect so-called "dissociated states," in which some brain areas display activity similar to wakefulness, while at the same time other regions show sleep patterns.[9-12] In transitional states, such as the falling- asleep process, state dissociation is particularly likely to occur. Indeed, several EEG studies suggest that the transition from wakefulness to sleep is not a spatially and temporally uniform process. Low-frequency EEG activity characteristic of sleep increases along an anterior-posterior axis[13-18] and displays interhemispheric differences in onset.[19] Recent work using functional MRI (fMRI) and intracerebral EEG recordings has revealed that subcortical and centrencephalic structures are deactivated before lateral cortical areas,[20-22] and that the contributions of spatially distinct nodes of the default mode network change during the transition from wakefulness to sleep.[23] Along the same lines, results from a recent study using intracerebral EEG recordings suggest that the thalamus and the hippocampus display sleep rhythms well before neocortical regions.[24]

Although measures of EEG power and of cortical activation have provided valuable insights into local changes that occur during the falling-asleep period, the study of individual slow waves and spindles—the electrophysiological hallmarks of nonrapid eye movement (NREM) sleep—may be particularly well suited to characterize the spatial and temporal dynamics of this process. In fact, little is known about how spindles and slow waves evolve upon falling asleep. We hypothesized that, similar to changes in power and cortical activation, slow waves and spindles would consistently appear in some cortical regions first and then in others. The goal of the study was to

Submitted for publication November, 2013
Submitted in final revised form March, 2014
Accepted for publication March, 2014
Address correspondence to: Giulio Tononi, MD, PhD, Department of Psychiatry, University of Wisconsin–Madison, 6001 Research Park Boulevard, Madison, WI 53719; E-mail: gtononi@wisc.edu

confirm this hypothesis by performing a refined analysis of slow waves and spindles in the falling-asleep process. For this purpose, we took advantage of high-density EEG (hd-EEG), a technique that combines the high temporal resolution of EEG with a spatial resolution that, upon source modeling, is roughly comparable to positron emission tomography (PET). In order to identify consistent patterns both within and among individuals, we used a multiple serial awakening paradigm[25] that allowed us to obtain multiple falling-asleep periods for each subject.

METHODS

Subjects

Six healthy volunteers (three males, age 28 ± 5.7 y [mean ± standard deviation]), range 21-38) screened for neurological, psychiatric, and sleep disorders and who were not on psychotropic medication participated in the study. All the subjects had a good sleep quality as assessed by the Pittsburgh Sleep Quality Index prior to enrolling (less than 5 points), and scored less than 10 points on the Epworth Sleepiness Scale. Written informed consent was obtained from each subject and the study was approved by the University of Wisconsin Institutional Review Board.

Procedure

This study was conducted as part of a larger research project assessing mental activity during sleep.[25] Six overnight recordings in the laboratory were scheduled for each subject. Participants were awakened at 15- to 30-min intervals, irrespective of sleep stage, and underwent a short interview lasting less than 4 min about their mental activity. Recordings were performed using hd-EEG with a 256-channel system (Electrical Geodesics, Inc., Eugene, OR), electro-oculography (four of the 256 electrodes placed at the outer canthi of the eyes were used to monitor eye movements) and submental electromyography (using the Electrical Geodesics polygraph input box). The EEG signal was sampled at 500 Hz. Recordings were filtered between 0.3 and 50 Hz and sleep scoring was performed over 30-sec epochs according to standard criteria[26] by a physician who is board certified in sleep medicine.

Definition of the Falling-Asleep Period

All the EEG recordings preceding the 529 awakenings performed in stages N2 and N3 were visually inspected. Two events, the end of alpha activity and the first slow wave sequence (FSS), were marked and used to define the beginning and the end of the falling-asleep period, respectively. The end of alpha activity was defined as the moment when continuous alpha activity characteristic of wakefulness was replaced by the high-frequency, low-voltage activity typical of stage N1. The FSS was defined as the first slow wave burst in the falling-asleep period consisting of more than two successive slow waves in the same derivation (duration of > 0.5 sec between consecutive zero crossings, > 75 μV peak-to-peak amplitude for each slow wave of the FSS) that were not followed by an arousal. The FSS generally appeared at the transition between stage N2 and N3. We chose this comparatively long time frame rather than one particular event (i.e., the first slow wave or sleep spindle) to define the falling-asleep period, in an attempt to capture the process in its entirety, from clearly defined wakefulness to well-established sleep. Although considerable controversy exists in the literature as to how define sleep onset, it can be said that by the end of stage N2, the major behavioral, EEG, physiological, and subjective changes characteristic of sleep have occurred.[27] The EEG signal corresponding to each falling- asleep segment (FAS) was extracted, including 30 sec before the end of alpha activity and 30 sec after the FSS. FASs containing major movement artifacts, long arousals (> 10 sec), shifts back toward lighter sleep stages, or in which subjects reached the end of alpha activity in less than 30 sec or were awakened before or within the 30 sec after the FSS were excluded from subsequent analysis. 141 FASs were retained (23.5 ± 5.9 per subject, length 9.3 ± 2.1 min, range 1-26 min, see also Table S1, supplemental material). They contained 9.0 ± 3.0 % of epochs scored as wakefulness, 12.1 ± 3.1 % of stage N1, 71.7 ± 4.0% of stage N2 and 5.9 ± 1.4% of stage N3.

Preprocessing of the EEG Signal

Bad channels were visually identified, rejected, and replaced with data interpolated from nearby channels using spherical splines (NetStation, Electrical Geodesics Inc.). Independent Component Analysis (ICA) was performed for each FAS to remove ocular, muscular, and electrocardiograph artifacts using EEGLAB routines.[28] Considering the relatively low number of data points in some of the short FASs, we performed Principal Component Analysis (PCA) before ICA to reduce the number of components to 128.[28] Only ICA components with specific activity patterns and component maps characteristic of artifactual activity were removed.[29] After excluding electrodes located on the neck/face region, the signal was re-referenced to the average of the remaining 185 channels.

Data Analysis

To compare FASs of different durations, we divided each FAS, starting from the end of alpha activity, into 10 time epochs of equal length.[30,31] The signal corresponding to the 30 sec before the end of alpha activity was used as a "presleep baseline."

To better characterize regional changes in the course of the falling-asleep period, we defined six regions of interest (ROIs), representing the medial anterior, medial posterior, left and right anterior, and left and right posterior brain areas. Because no evident differences emerged between left and right ROIs in all examined conditions, and in order to simplify the presentation of results, we merged them obtaining a lateral anterior ROI and a lateral posterior ROI. To determine how power, slow wave, and spindle characteristics changed in the course of the 10 epochs, we computed average values of the parameters of interest between homologous time epochs of different FASs for each channel. For ROI based analyses, we calculated the average across the channels included in the ROI.

EEG Spectral Analysis

For each FAS and EEG channel, power spectral density estimates were computed by fast Fourier transform in 2-sec Hamming windows to obtain a 0.5 Hz bin resolution. Adjacent frequency bins were then collapsed in order to obtain the following EEG bands: delta (1.0-4.5 Hz), theta (4.5-7.5 Hz), alpha (8.0-12 Hz), sigma (11-15 Hz), high beta (20-25 Hz) and low

gamma (25-40 Hz). We averaged the power spectra across frequency bins within each of the 10 time epochs, and computed the ratio between each epoch and the corresponding presleep baseline. For each subject, the average ratio between homologous epochs of different FASs was calculated for each frequency bin, channel, and previously defined ROI.

Analysis of Slow Waves

Slow Wave Detection: An automatic detection algorithm, adapted from a previous study,[32] was used for slow wave detection. EEG signals from each electrode were referenced to the average of the two mastoid electrodes and then downsampled to 128 Hz and band-pass filtered (0.5-4.0 Hz, stop-band at 0.1 and 10 Hz) using a Chebyshev Type II filter (Matlab, The Math Works Inc, Natick, MA). Only slow waves with a duration of 0.25-1.0 sec between consecutive zero crossings and a maximum peak-to-peak amplitude greater than 75 μV were considered. For all the detected slow waves, the following parameters were determined: number, timing, duration, peak-to-peak amplitude, number of positive and negative peaks, slope 1 (between the first zero crossing and the negative peak), and slope 2 (between the negative peak and the second zero crossing).

Source Localization, Probabilistic Origins, and Involvement: To create a single timing reference for source localization, a similar wave detection procedure was applied to a composite reference signal generated from all mastoid referenced channels post-ICA. The negative-going reference envelope was generated by selecting the fifth most negative sample across all channels and then the resulting signal (0.5-40 Hz, stop-band at 0.1 and 60 Hz) underwent broadband filtering prior to wave detection. This method facilitates the detection of both local and global slow waves. Reference slow waves were detected as previously mentioned except that an amplitude criterion of 40μV was applied only to the maximum negative amplitude of the envelope. Source localization of slow waves was performed on filtered data (0.5-4 Hz, 256 electrodes, 2 sec surrounding the negative peak of the reference slow waves) using the GeoSource tool (NetStation, Electrical Geodesics, Inc). A four-shell head model based on the Montreal Neurological Institute atlas and a standard coregistered set of electrode positions were used to construct the forward model. The inverse matrix was computed using the standardized low-resolution brain electromagnetic tomography (sLORETA) constraint, and a Tikhonov regularization procedure was applied to account for the variability in the signal-to-noise ratio.[33] The source space was restricted to 2,447 dipoles distributed over 7 mm^3 cortical voxels. The relative current was calculated by dividing the inverse model of each slow wave by the average of the last 5 sec of source modeled signal in the presleep baseline of the same FAS (similar results were obtained without baseline correction). For each subject we determined the probabilistic origin and involvement values as previously described.[34] Briefly, the probabilistic origin was defined as the probability for a specific voxel to represent the potential origin of a slow wave. Specifically, the origin of an individual slow wave in source space was represented by the top 10% of voxels, which showed the earliest relative current maxima, identified within a time-window of 100 ms centered on the negative voltage peak of the slow wave (a threshold corresponding to 25% of the maximum relative current value was also applied). Cortical involvement was defined as the average of the relative current achieved within the same time-window. For each subject and epoch of the FAS, we computed the mean probabilistic origin and involvement value for all the voxels. To compare results obtained in different epochs and subjects, for both parameters we computed the ratio between the value in each voxel and the value resulting from the average of all brain voxels.

Relationship Between Slow Waves and Gamma Power: Considering the reported association between gamma activity and specific phases of the cortical slow wave,[35] we next examined the temporal relation between gamma and delta power during the period centered on the negative peak of the slow wave. For each wave detected in early (epochs 2 and 3) and late epochs (epochs 8 and 9) in a single frontal channel (Fz), we computed the root mean square (RMS, 31.25 ms time-window) of the delta (0.5-4 Hz) and gamma (30-50 Hz) power for the 10 sec before and after the negative peak of the wave. For each subject, delta and gamma RMS time series were z-score transformed and averaged across all the detected slow waves. A group average was computed on the 1.5 sec centered on the negative peak of the slow wave for a comparison between slow waves occurring in early and late epochs of the falling- asleep period.

Analysis of Sleep Spindles

Sleep Spindle Detection: An automatic algorithm, adapted from a previous study,[36] was used for spindle detection and analysis. For each FAS, the average-referenced signal was downsampled to 128 Hz and band-pass filtered between 12 and 15 Hz (-3 dB at 11 and 15 Hz). The following parameters were determined for all the detected spindles: number, timing, duration, maximal amplitude, and frequency. Based on previous studies,[4,37,38] spindles were categorized as fast centroparietal spindles or slow frontal spindles. Because spindle frequency varied considerably among subjects, we used an individualized threshold to separate these two types of spindles. For each participant, the threshold was defined as the intermediate value between the average spindle frequency in one centroparietal (Pz) and one frontal (Fz) channel. Spindles associated with slow waves were identified using the information obtained from the automated detection procedures. Specifically, for each channel and for each of the 10 epochs of all FASs, we identified all spindles that either ended within the 150 ms before or started within the 150 ms after the slow wave negative peak, and stored their properties for subsequent evaluations and comparisons. Spindles preceding and following the negative peak were analyzed separately, based on previous work[39] suggesting a specific association between low-frequency (slow) spindles and the negative slope of the slow wave (slope 1), and between high-frequency (fast) spindles and the positive slope of the slow wave (slope 2).

Spindle Synchronization: To investigate how the proportion of local and diffuse spindles changed during the FAS, we calculated the scalp involvement for each spindle detected in a frontal reference channel (Fz) in all the FAS epochs. For each spindle we computed the number of synchronous detections in all other electrodes and expressed the scalp involvement as the mean percentage of channels showing a synchronous

spindle during each epoch. Spindles were considered synchronous with the reference spindle if either the starting times were separated by less than 200 ms or the half-spindles were separated by less than 400 ms. A repeated-measures analysis of variance (ANOVA) (subject × epoch) was used to assess a significant effect of epoch on the level of spindle diffusion across the scalp.

Source Localization, Probabilistic Origins, and Involvement: Source localization was computed on the filtered (11-15 Hz) signal (256 channels) using the same procedures previously described for slow waves. Source analysis was performed for fronto-central (identified in the Fz channel) and centroparietal spindles (identified in the Pz channel) separately, minimizing any overlap by excluding all events simultaneously detected in both channels. For each subject, we determined the probabilistic origin as defined by the top 10% voxels that showed the earliest relative current maxima after the beginning of the spindle. Only relative current maxima above a threshold of 50% of the absolute maximum identified across all dipoles were included in this analysis. Involvement values were computed for each voxel by averaging the relative current achieved during the whole duration of the spindle. Parameters for spindle source localization were otherwise computed in the same manner as slow waves.

Statistical Analysis

If not stated otherwise, analyses were performed for each subject separately. Given the overall consistency of results among subjects and to simplify presentation of the results, we presented group-averaged results in the figures. When results in one or more subjects differed substantially from the averaged result, we indicated this in the text.

To compare slow wave and spindle characteristics between early and late epochs of the falling- asleep periods, we performed unpaired *t*-tests for each subject, comparing the parameter of interest across all the slow waves or spindles detected in each phase. We then carried out a conjunction analysis for all channels. Channels in which the P value was smaller than 0.05 in at least five of the six subjects were considered as significant.[34] To compare the probabilistic origin and involvement of slow waves and spindles between early and late epochs, and for other comparisons carried out at the group level, we performed voxelwise, paired nonparametric tests (Wilcoxon signed-rank test) on the mean values obtained for each subject.

RESULTS

Power Analysis

Topographical and regional power changes for different frequency bands are shown in Figures S1 and S2 (supplemental material), respectively. In the delta and theta frequency bands (1-7.5 Hz), spectral power increased progressively, earlier and more prominently in the anterior and medial brain regions than in the posterior and lateral regions. A transient decrease across epochs 5 to 7, which was most prominent in the anterior medial regions, was observed in five of the six subjects. For the alpha and sigma frequency bands (8-15 Hz), overall power decreased slightly in the first epoch with respect to the presleep baseline and then increased linearly. Sigma power also increased earliest and to the greatest extent in the anterior regions, but did not show a clear dissociation in the mediolateral dimension. Power in the high beta band (20-25 Hz) showed considerable variability, both within and between subjects. After a marked decrease following the presleep baseline, high beta power remained stable in two subjects and showed a progressive increase in four subjects. Gamma activity (25-40 Hz) decreased progressively in all participants after the end of alpha activity, without displaying a consistent regional gradient.

Slow Wave Analysis

Slow Wave Characteristics

In agreement with the results of the power analysis in the delta range, the analysis of individual slow waves revealed a characteristic time course of the number and amplitude of slow waves in the falling-asleep period. In all the subjects, the number of slow waves at first increased, earliest and most prominently in anterior medial brain regions, followed by other regions (Figure 1A and 1B). This rapid initial increase was then followed by a slight decrease or a plateau across epochs 2 and 5. Finally, by epoch 8 at the latest, the number of slow waves began to increase again. This pattern was particularly marked in the anterior medial region in all the subjects. In five of the six subjects, the amplitude of slow waves also increased at the beginning of the falling-asleep period, reaching a peak somewhere between epochs 2 and 6, again most evident in the anterior medial region (Figure 1A and 1B). Subsequently, however, the amplitude of slow waves decreased. In one subject, slow wave amplitude was highest in the first epoch and then decreased progressively.

The distinct courses of slow wave amplitude and number (Figure 1B) indicated that the early phase of the falling-asleep period was characterized by relatively isolated, large-amplitude slow waves, whereas in the late phase numerous small-amplitude slow waves prevailed. The transient dip in delta power between epochs 5 and 7 (Figures S1 and S2) corresponded to the moment when slow wave amplitude decreased and slow wave number had not yet increased. To quantify and topographically map these changes, we directly compared characteristics of slow waves in early epochs (epochs 2 and 3) with slow waves in late epochs (epochs 8 and 9). As shown in Figure S3 (supplemental material), the amplitude and slope of slow waves detected in early epochs were significantly larger in the frontal region, whereas the number of negative peaks was smaller than for slow waves detected in late epochs. Slow waves detected in early epochs also tended to have a longer duration and more positive peaks compared slow waves detected in late epochs in this region, but these differences were not significant, based on our criteria.

Slow Waves and Gamma Power

Gamma activity is known to change in relation to specific phases of the cortical slow wave.[35] We therefore examined the time course of gamma and delta power during the period centered on the negative peak of the slow wave (Figure S4, supplemental material). Gamma power was high about 500 ms before the negative peak of the slow wave, then decreased approximately 250 ms before the negative peak, and started to increase

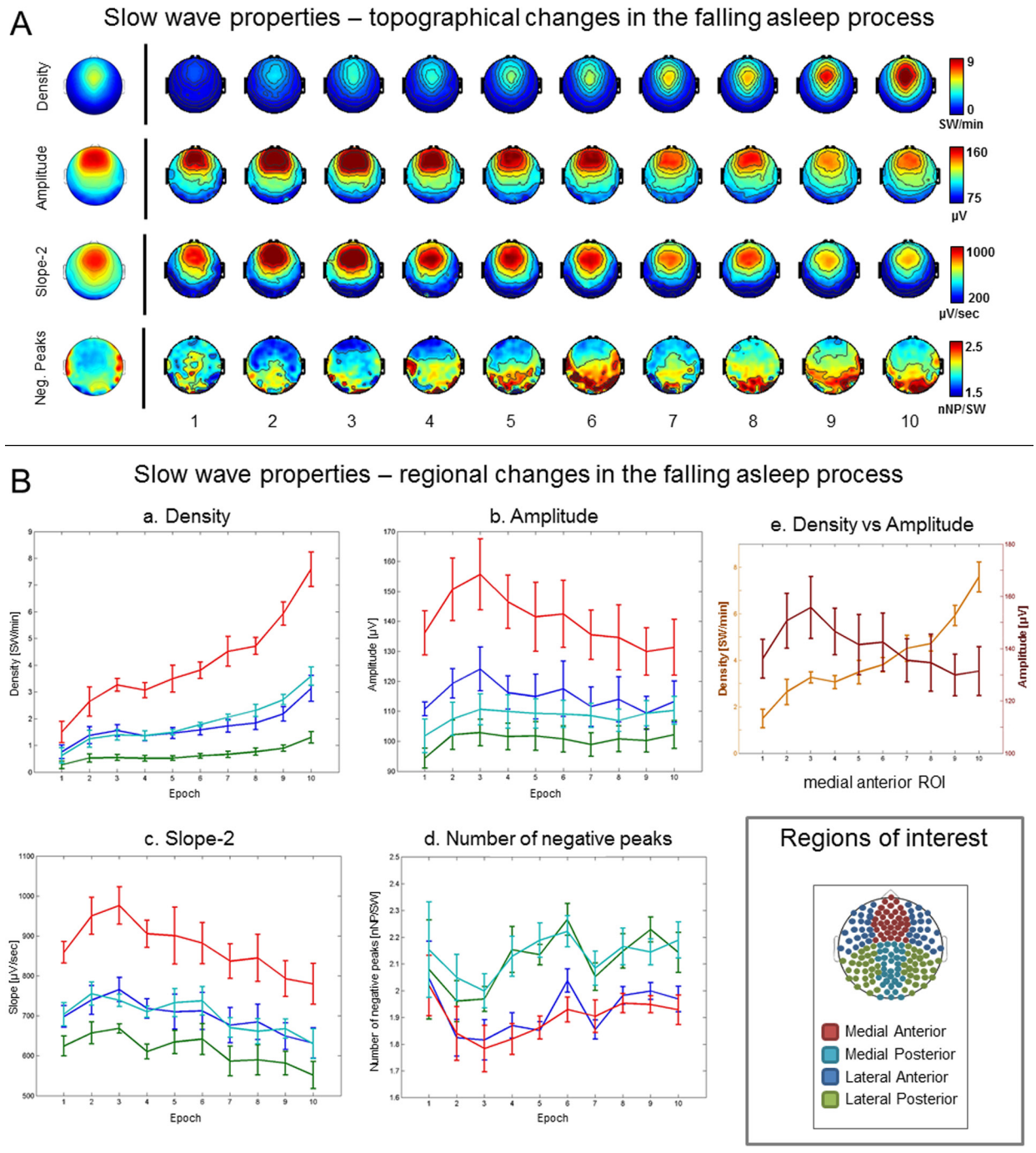

Figure 1—Slow waves: regional changes. **(A)** Topographical changes in slow wave density (slow waves per min [SW/min], first row), amplitude ([µV], second row), slope-2, corresponding to the slope of the negative to positive deflection of the slow wave ([µV/min], third row) and number of negative peaks per wave ([nNP/SW], fourth row) for the 10 consecutive epochs of the falling asleep period (group average). The images on the left of the black vertical line show the topographical distribution of the same characteristics obtained when considering the falling asleep period as a whole. **(B)** Evolution of slow wave density (a), amplitude (b), slope-2 (d) and number of negative peaks (e) for the four regions of interest (ROI) and 10 consecutive epochs of the falling asleep period (group average). Both amplitude and number are plotted on the same graph for the medial anterior ROI only (e). The small panel on the bottom right corner shows the ROIs used for analysis.

again just before the negative peak, reaching a maximum approximately 500 ms later. Gamma power thus reached its lowest value during the slow wave phase corresponding to the intracellular down state.[35,40] Slow waves detected in early epochs were associated with more pronounced and rapid changes in gamma power compared to slow waves detected in late epochs. This led to a significant effect at the group level (P = 0.03, signed rank test) within the 250 ms following the wave negative peak.

Origin and Involvement of Slow Waves (Source and Scalp Level)

To determine whether the origin of slow waves changed in the course of the falling-asleep period, we calculated, for

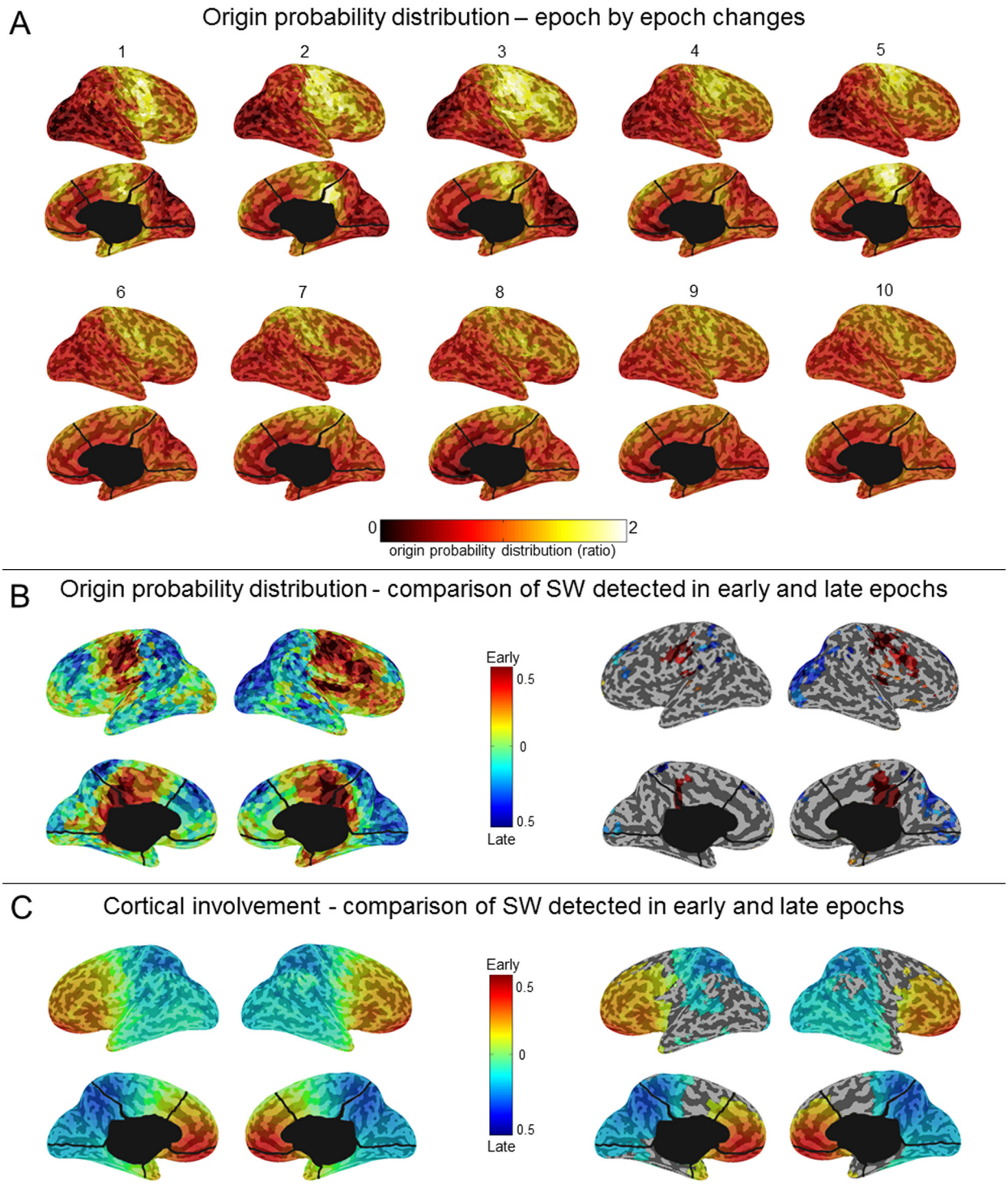

Figure 2—Slow waves: origin and involvement in source space. **(A)** Group averaged probabilistic distribution of slow wave origins shown on inflated cortical maps for each of the 10 consecutive epochs of the falling-asleep period. The probabilistic origin was defined as the probability for a specific voxel to represent the potential origin of a slow wave (top 10% voxels, which showed the earliest relative current maxima). To be able to compare results obtained in different epochs and subjects, we computed the ratio between the value in each voxel and the value resulting from the average of all brain voxels. **(B)** Inflated cortical maps of differences in probabilistic origins between slow waves detected in early and late epochs (left). Only areas that significantly differed between slow waves detected in early and late epochs are shown (signed rank test, $P < 0.05$; right). **(C)** Inflated cortical maps of differences in involvement between slow waves detected in early and late epochs (left). Involvement was defined as the average of the relative current achieved within a time-window of 100 ms centered on the negative voltage peak of the slow wave. Only areas that significantly differed between slow waves detected in early and late epochs are shown (signed rank test, $P < 0.05$; right).

each slow wave in the 10 time epochs, which voxels were most likely to be at the origin of that wave.[34] Figure 2A shows that the most frequent origins of slow waves detected in early epochs were localized to a region encompassing the primary sensory and motor cortices (extending to the lateral prefrontal cortex on the right side), the inferior frontal gyrus\insula, and the posteromedial parietal cortex (posterior cingulate and precuneus). Although these preferential origins predominated over the whole course of the falling-asleep period, the relative contributions of other brain regions (in particular the right lateral prefrontal cortex, and the lateral parietal, lateral temporal, and occipital areas) increased in the later phase of the FASs (Wilcoxon signed-rank test at the group level, $P < 0.05$; Figure 2B, see also Figure S5, supplemental material). In other words, the origins of slow waves became more evenly distributed over the cortex during the latter part of the falling-asleep period. We then evaluated the amount of current produced by different cortical areas during slow waves (cortical "involvement"[34]) detected in early and late epochs separately. Compared with slow waves in late epochs, slow waves in early epochs involved preferentially the frontal region, in particular the medial part. By contrast, slow waves detected in late epochs involved the parietal, temporal and occipital regions to a greater extent than slow waves detected in early epochs ($P < 0.05$) (Figure 2C). A similar analysis performed at the scalp level confirmed that slow waves in early epochs tended to involve broad regions of the cortex, whereas slow waves in late epochs involved relatively circumscribed cortical areas (illustrative examples are shown in Figure 3). A summary of typical, distinctive characteristics of slow waves detected in early and late epochs of the falling-asleep period is provided in Table S2 (supplemental material). Visual inspection and analysis of individual slow waves confirmed that these distinctive characteristics are indeed typical of the majority of slow waves detected early and late. Nevertheless, some waves in the early epochs displayed the characteristics typical of slow waves of the late epochs, such as a small amplitude, and *vice versa*.

To exclude that differences in slow wave origin and involvement between slow waves in the early and late epochs were caused by the presence of vertex waves in early epochs, we performed a separate analysis for slow waves with a duration between 0.1-0.25 sec, a range that is typical for vertex waves.[41] This analysis showed specific origins and involvements of vertex waves that were distinct from those observed for slow waves detected in early epochs (Figure S6, supplemental material). In particular, the involvement of vertex waves was more posterior compared to that of slow waves detected in early epochs.

Spindle Analysis

Spindle Characteristics

The number of spindles increased initially in all subjects and then decreased after the ninth epoch at the latest (Figure 4A and 4B). The increase was particularly marked and appeared earlier in anterior brain regions in comparison with posterior ones. The duration of spindles showed a similar course in all subjects. After an initial steep increase in spindle frequency between the first and second epoch, a gradual decrease was observed in all subjects in the course of the falling- asleep period. The steep increase in frequency between epochs 1 and 2 (shown in Figure 4A and 4B) involved mainly the posterior brain regions, probably reflecting the disappearance of very short bursts of alpha activity. Indeed, upon visual inspection, low frequency, spindle-like oscillations were identified in the first segment of the falling-asleep period. Our results confirm the topographical distinction between faster centroparietal and slower frontal spindles[42,43] (Figure 4A). Frontal spindles showed a tendency to appear before centroparietal spindles, although this difference in latency was significant in only two subjects (data not shown), consistent with results of a recent study.[44] Figure 4A and 4B show that spindle frequency in both frontal and centroparietal regions decreased in the falling-asleep period, but to a greater extent in the frontal region. When directly comparing spindle frequency between early and late epochs (Figure S7, supplemental material), a significant decrease was observed only in the frontal region. In the same frontal regions late spindles tended to be longer, but this effect was not significant. As for spindle amplitude, it showed a tendency to be lower in late spindles. This effect was significant for one frontal electrode.

Scalp Involvement of Sleep Spindles

We then examined, at the scalp level, how many channels were involved in each spindle in the course of the falling-asleep period—an index of how widespread spindles were in each epoch. The proportion of channels involved was relatively low (20% ± 11%) early in the falling-asleep period, but then increased progressively, reaching a maximum between epochs 4 and 6 in all subjects (44.8% ± 1.7% in epoch 5; Figure 4C). Involvement then remained relatively stable, showing only a slight reduction at the end of the FAS. Repeated-measures ANOVA confirmed the existence of a clear epoch effect ($P < 5*10^{-11}$). The degree of scalp involvement positively correlated with spindle amplitude ($P < 10^{-27}$ in all subjects, $n = 724.3 \pm 384.3$) and duration ($P < 10^{-4}$ in all subjects), whereas no correlation was found for spindle frequency.

Origin and Involvement of Sleep Spindles at the Source Level

Sleep spindles are generated in the thalamus, via the interaction between thalamic reticular and thalamocortical cells,[2] and amplified in the cortex.[45] Thalamic activity could not be directly assessed in the current study. Instead, we investigated which cortical areas first showed spindle-related activity ("origins" of spindles). The characteristics of cortical spindles appear to reflect important properties of spindle generation at the level of thalamic cells.[4] The probabilistic origin was calculated for frontal as well as for centroparietal spindles, both in early and late epochs. The most frequent origins (top 10%) of frontal spindles were the anterior cingulate cortex and the dorsolateral and medial prefrontal cortex, whereas centroparietal spindles most frequently originated in the precuneus and posterior cingulate cortex (Figure S8, supplemental material). In the course of the FAS, the relative proportion of posteromedial parietal origins increased for frontal spindles, whereas the relative contributions of frontal origins increased for centroparietal spindles, (Wilcoxon signed-rank test at the group level,

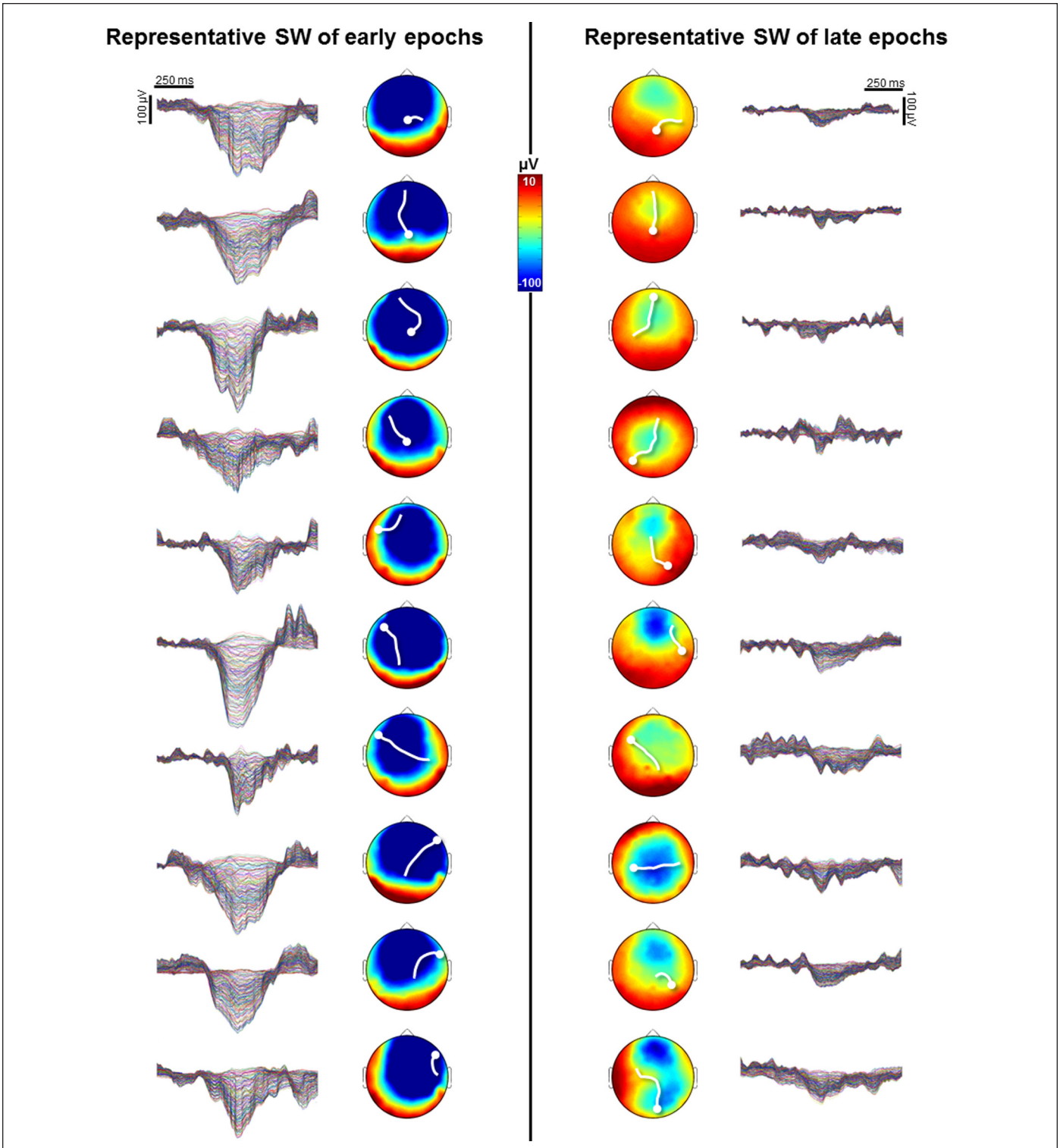

Figure 3—Scalp involvement, origin, and propagation for representative slow waves (SW) of early and late epochs in one subject (S2). Slow waves detected in early epochs have a large amplitude and involve broader parts of the cortex when compared to slow waves detected in late epochs. In addition, slow waves detected in early epochs originate predominantly from a limited number of hotspots, whereas the origins of slow waves detected in late epochs are more evenly distributed over the cortex. The scalp involvement was defined as the average of current achieved during a 100 ms window around the negative peak of the electroencephalographic (EEG) slow wave (shown on the left and on the right for slow waves detected in early and late epochs respectively—185 channels). Scalp origins were determined using an algorithm similar to one that was previously described.[32,34,106] Briefly, we determined for each EEG channel whether a negative peak was detected on the band-pass filtered signal within ± 200 ms of the reference wave peak. The timing of each involved channel's EEG peak was used to create a rectangular delay map grid with centimeter resolution based on electrode positions. A streamline tangential to the instantaneous velocity direction in the two-dimensional vector field of delays was determined for each involved electrode. The streamline for an individual electrode progressed in both directions along the vector field (up and down the gradient). The beginning of the longest streamline was considered the origin of the wave.

P < 0.05; Figure 5A and 5B). Similarly, early centroparietal spindles were characterized by a greater relative involvement of occipital, parietal, temporal, and insular areas, whereas late centroparietal spindles showed a higher involvement over the fronto-medial region (P < 0.05) (Figure 5C). No such difference in the degree of involvement was observed for frontal spindles.

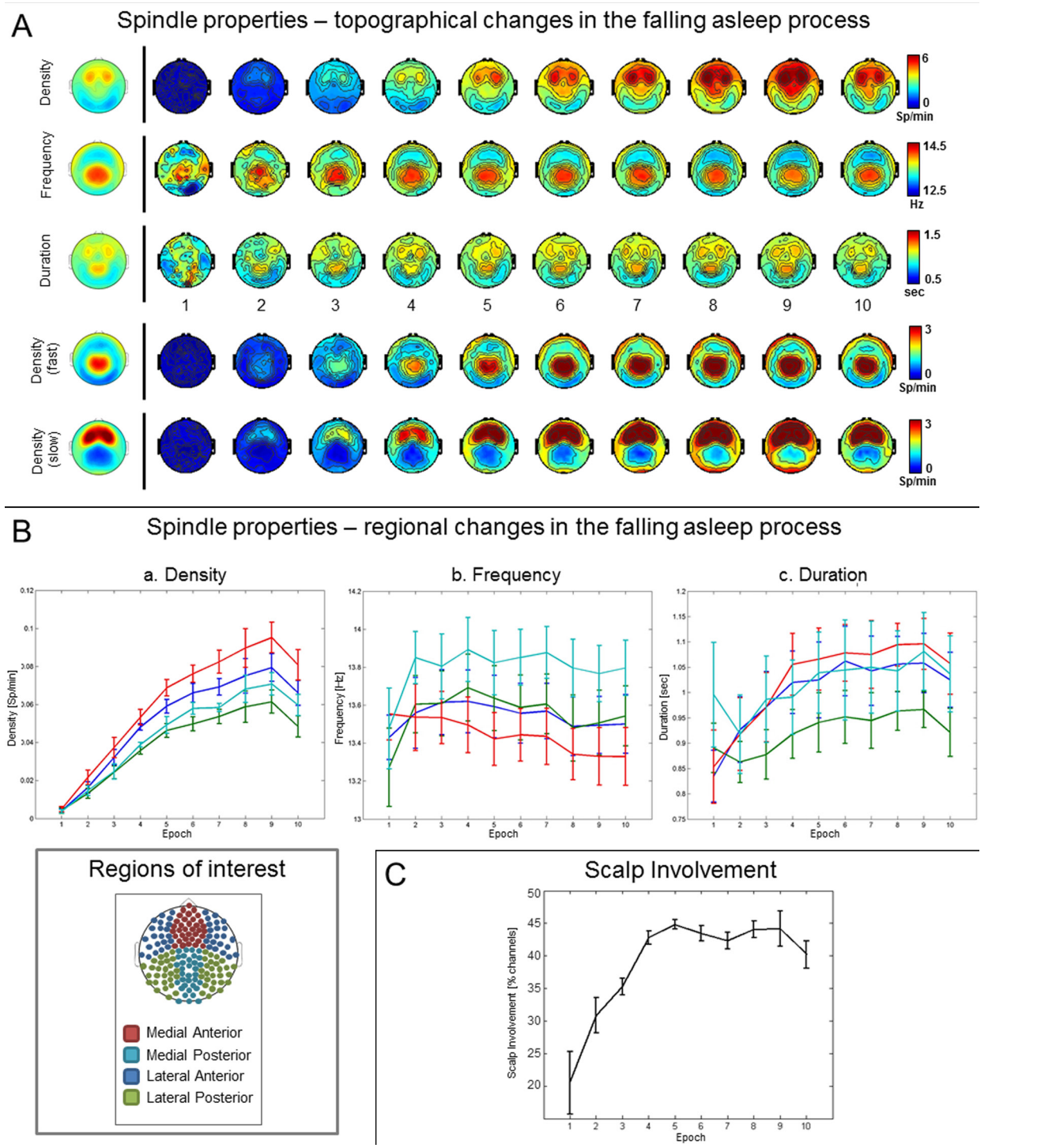

Figure 4—Spindles: regional changes and scalp synchronization. **(A)** Topographic changes in spindle density (spindles per min [Sp/min], first row), frequency ([Hz], second row) and duration ([sec], third row) for the 10 consecutive epochs of the falling asleep period (group average). The fifth and sixth rows show the topographic changes in fast and slow spindle density, respectively. The images on the left of the black vertical line show the topographical distribution of the same characteristics obtained when considering the falling asleep period as a whole. **(B)** Evolution of density (a) frequency (b) and duration (c) of spindles in the four regions of interest (ROI) for the 10 consecutive epochs of the falling asleep period (group average). The small panel on the bottom left corner shows the ROIs used for analysis. **(C)** Proportion of channels involved for each spindle detected in the reference channel across the 10 time epochs of the falling-asleep period. For each spindle we computed the number of synchronous detections in all other electrodes and expressed the scalp involvement as the mean percentage of channels showing a synchronous spindle during each epoch. Spindles were considered synchronous with the reference spindle either if the starting times were separated by less than 200 ms or if the half-spindles were separated by less than 400 ms.

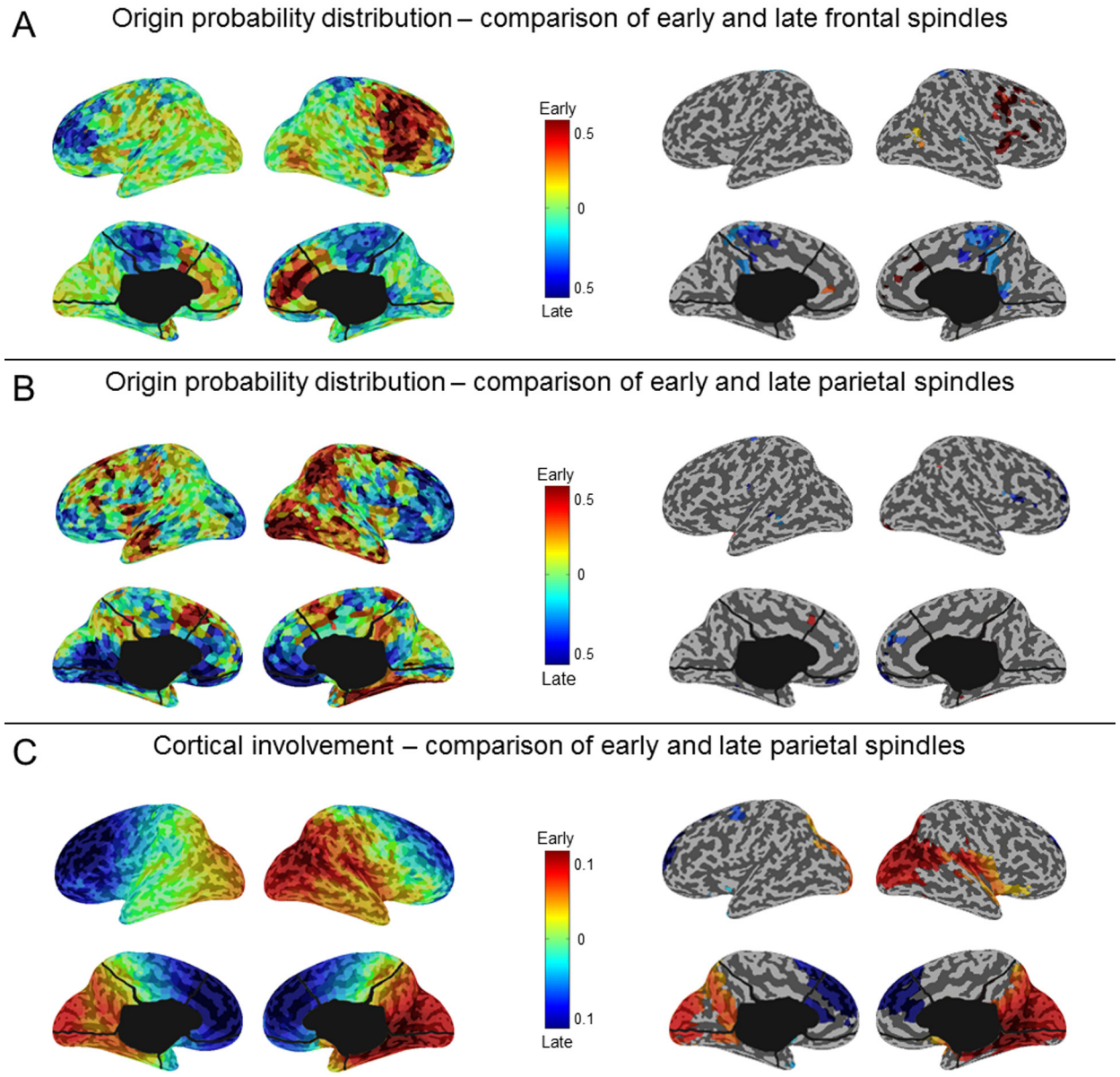

Figure 5—Spindles: origin and involvement in source space. **(A)** Inflated cortical maps of differences in probabilistic origins between early and late phase frontal spindles (left). Only areas that significantly differed between early and late phase frontal spindles are shown (signed rank test, $P < 0.05$; right). The probabilistic origin was defined as the top 10% voxels, which showed the earliest relative current maxima after the beginning of the spindle. Only relative current maxima above a threshold of 50% of the absolute maximum identified across all dipoles were included in this analysis. **(B)** Inflated cortical maps of differences in probabilistic origins between early and late phase parietal spindles (left). Only areas that significantly differed between early and late phase parietal spindles are shown (signed rank test, $P < 0.05$; right). **(C)** Inflated cortical maps of differences in involvement between early and late phase parietal spindles (left). Only areas that significantly differed between early and late phase parietal spindles are shown (signed rank test, $P < 0.05$; right). For each voxel, spindle involvement was defined as the average relative current achieved in the whole duration of the spindle.

The Relation Between Slow Waves and Spindles

Across all channels, 2.2% (± 0.76%) of detected slow waves were characterized by the presence of a spindle on the negative slope (prepeak), whereas 3.4% (± 1.3%) were associated with a spindle on the positive slope (postpeak). The probability for a slow wave to be associated with a spindle was highest in frontal regions for both prepeak and postpeak spindles (Figure S9A, supplemental material). In line with previous work, postpeak spindles tended to show a higher frequency when compared to prepeak spindles (Figure S9C), this effect was significant in frontal electrodes at the group level ($P < 0.05$, uncorrected). For both types of spindles, the incidence, as expressed by the association probability value, mirrored the general course of spindles described previously: it increased during the first half of the falling-asleep period, reached a maximum in the central part, and then decreased during the last epochs (Figure S9B). Spindles associated with slow waves detected in early epochs showed a trend toward a higher frequency and shorter duration when compared with spindles associated with slow waves detected in late epochs (data not shown), again in line with the general changes described for spindles.

When considered together, the course of slow waves and spindles in the falling-asleep period can be divided into three parts (Figure 6): (1) In the first third of the falling-asleep period, slow wave and spindle densities increase sharply and almost in parallel. (2) In the second part, both slow waves and spindles increase in number but follow different courses: slow wave density decreases or remains stable, and then slowly increases, whereas spindle density continues to increase linearly. (3) In the last 10% of the falling-asleep period, slow waves and spindles show an opposite course: slow wave density rises steeply, while spindle density decreases.

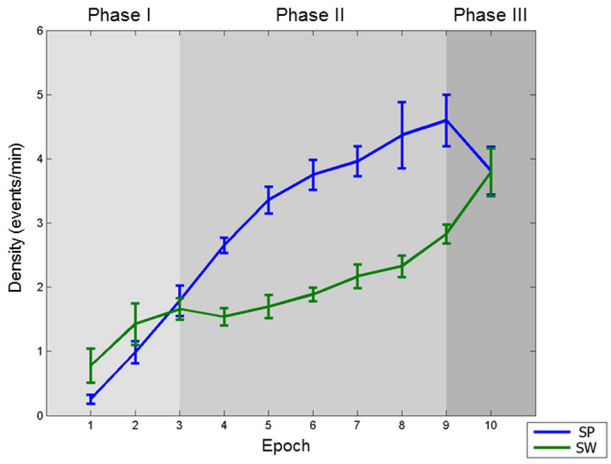

Figure 6—The three phases of the falling-asleep period. Spindle (SP) and slow wave (SW) densities (events per min) in the course of the 10 consecutive epochs of the falling-asleep period (group average). Three phases can be identified, as described in the main text: Phase I: slow wave and spindle densities increase sharply and almost in parallel; Phase II: both slow waves and spindles increase in number but follow different courses: slow wave density slightly decreases or remains stable, and then slowly increases, whereas spindle density continues to increase linearly; Phase III: slow waves and spindles show an opposite course: slow wave density rises steeply, whereas spindle density decreases.

DISCUSSION

Slow Waves in the Falling-Asleep Period

The EEG slow wave of NREM sleep reflects a slow oscillation of thalamocortical neurons between two states, each lasting a few hundred milliseconds[46-50]: (1) a state during which neurons are depolarized (up state) and display a high firing rate (on state), and (2) a state characterized by intracellular hyperpolarization (down state) and relative neuronal quiescence (off state). Specifically, the positive-to-negative deflection of the EEG slow wave corresponds to the down state recorded intracellularly, and to the off state detected extracellularly.[49,51] The propensity of thalamocortical neurons to fall inevitably into a silent, hyperpolarized down state after a period of activation, also termed bistability, reflects a fundamental characteristic of the cortex during NREM sleep. Although it has been suggested that thalamic oscillators may play a role in this slow oscillation,[52] it is now established that the cortex alone is necessary and sufficient to generate and sustain slow waves.[53,54] A recent study, in which scalp EEG, intracerebral EEG, and unit firing were recorded simultaneously in multiple brain regions of patients with epilepsy,[3] confirmed that in humans, the slow wave reflects the same alternation between neuronal firing and silence previously described in animals. The study also showed that, especially toward the end of the night, the slow oscillation can occur locally, meaning that some brain regions can be in the on state, whereas simultaneously other brain regions are silent. In addition, it was demonstrated that small amplitude slow waves in the EEG mostly represent local waves, occurring out of phase across different brain regions, as opposed to large amplitude "global" EEG slow waves that are in phase across different brain regions. In the current work, we used the same criteria to define and detect slow waves, that is, their negative peak, knowing that it corresponds to the end of the off state. Unlike the previous study, we focused specifically on the falling-asleep period and used hd-EEG as a noninvasive technique. Without any *a priori* assumption, we found that in the transition to sleep, the number and amplitude of slow waves followed two dissociated, intersecting courses: slow wave number increased slowly at the beginning and rapidly at the end of the falling-asleep period, whereas slow wave amplitude at first increased rapidly and then decreased linearly. Slow waves occurring early in the falling- asleep period tended to be infrequent and had a large amplitude, a steep slope and few negative peaks. They involved broad parts of the cortex, predominated over frontomedial regions and were first detected in a region encompassing the primary motor and sensory cortices, the posteromedial parietal cortex and the insular area. Most slow waves occurring in the later part of the falling- asleep period had a smaller amplitude and slope as well as a higher number of negative peaks compared to slow waves occurring early. They also tended to involve more circumscribed parts of the cortex and could originate from any part of the cortex.

The region in which slow waves tended to originate, especially at the beginning of the transition to sleep, overlaps with slow wave hotspots identified during established sleep by other studies using source modeling[34] and fMRI acquisitions phase-locked to slow waves.[55] The sensorimotor cortex, a primary hotspot in our study, also constitutes a preferential site for triggering slow waves with transcranial magnetic stimulation (TMS) during sleep.[56] In fact, the slow waves induced by TMS over this region share a number of similarities with slow waves detected early in the falling-asleep period, including a large amplitude, a frontal distribution and a diffuse cortical involvement. It thus appears that some brain regions are more prone than others to give rise to slow waves, especially in the early part of the falling-asleep period, but also during established sleep. Why these areas should show such a propensity to produce slow waves is currently unknown. Interestingly, the preferential region of origin identified in the current work contains the highest degree of noradrenergic innervation in the human and monkey cortex,[57-59] suggesting that especially slow waves occurring early in the falling-asleep period may be functionally and anatomically related to arousal systems. In agreement with this observation, a recent fMRI study found significant activations in the pontine area encompassing the locus coeruleus specifically during high amplitude slow waves in sleep.[55] A functional interaction between the locus coeruleus and prefrontal cortical neurons has also been suggested by a recent study carried out in naturally sleeping rats, which

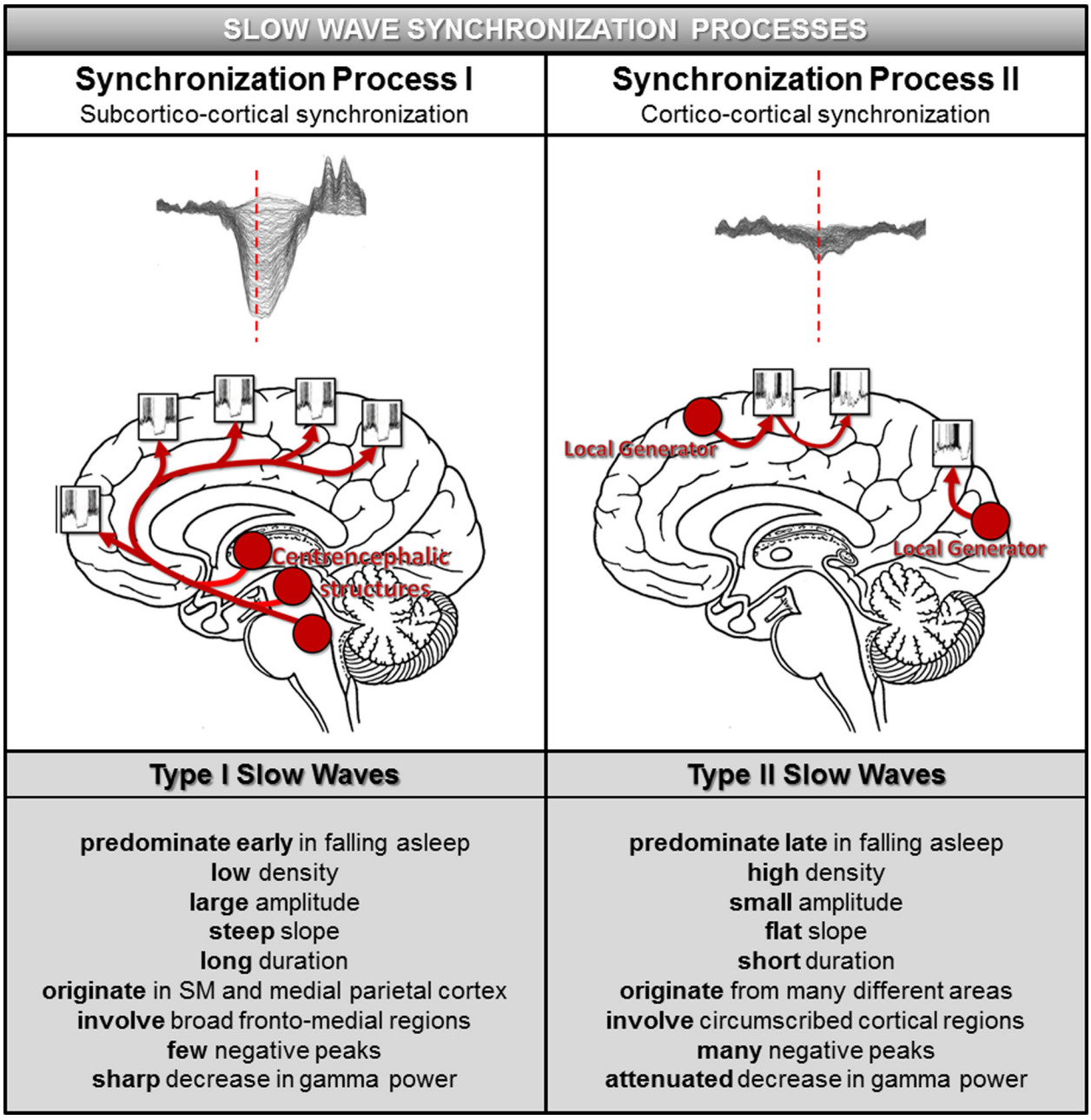

Figure 7—Model of slow wave synchronization involving two processes. According to this model, slow waves in the transition to sleep are synchronized by two distinct processes. Synchronization Process I, underlying type I slow waves, operates in a bottom-up manner through subcortical projections to the cortex originating in arousal-related structures (left upper panel). The subcortical location and wide-spread nature of these projections result in a particularly fast and effective synchronization, giving rise to slow waves that display the characteristics outlined in the left lower panel. Synchronization Process II, associated with type II slow waves, represents a corticocortical (horizontal) synchronization. This type of synchronization is likely to be less efficient, as a cortical region can reach only a limited amount of neuronal populations at the same time, resulting in slow waves that have the features outlined in the right lower panel. SM = sensorimotor cortex.

showed specific firing of locus coeruleus neurons during specific phases of the cortical slow wave.[60] The fact that the slow wave hotspots, which are heavily innervated by the arousal- and wakefulness-promoting neurotransmitter noradrenaline, are also among the first ones to give rise to sleep-promoting slow waves seems paradoxical, but may be accounted for by a specific, arousal-related mechanism of slow wave synchronization outlined in the next paragraphs.

Possible Neuronal Synchronization Mechanisms Underlying Type I and Type II Slow Waves

When neurons are stimulated in a bistable state (NREM sleep), for example, by TMS[56] or intracortical electrical stimulation,[61] they simultaneously undergo a stereotypical down state, resulting in the EEG slow wave. Evidence from large scale computer simulations,[62] local field potential studies of slow waves in the rat[51,63] and EEG studies in humans[32]

suggests that the amplitude, number of negative peaks, and slope of the slow wave reliably reflect the degree and speed of synchronization across neuronal populations. Specifically, steep, high-amplitude slow waves with few negative peaks result from a fast and efficient neuronal synchronization involving a large number of neurons.[32,51,63] The fact that slow waves occurring early in the falling-asleep period and those that occur later differ in precisely these parameters suggests that they may result from distinct synchronization mechanisms (Figure 7).

We hypothesize the existence of two slow wave synchronization processes in the transition to sleep:

(1) Synchronization Process I, a "bottom-up," common input synchronization mechanism mediated by subcortical, arousal-promoting structures, which predominates early in the falling-asleep process. Slow waves resulting from this synchronization process, which will be called "type I" slow waves, are typically large, steep, originate predominantly in the sensorimotor region and the posteromedial parietal cortex and involve a broad frontomedial region that falls asleep first.

(2) Synchronization Process II, a "horizontal" synchronization mechanism mediated by cortico-cortical connections, which predominates later when sleep is more established. Slow waves resulting from this synchronization process, which will be called "type II" slow waves, are typically smaller, less steep, originate anywhere in the cortex, and involve circumscribed cortical areas including posterior and lateral brain regions, which fall asleep later.

The characteristic features distinguishing type I and type II slow waves and their proposed synchronization mechanisms are outlined in Figure 7. It should be emphasized that, although type I and type II slow waves are typical of the early and late falling-asleep process, respectively, visual inspection of individual waves showed that slow waves matching type I criteria can occur late, and slow waves matching type II criteria can occur early. An automated, classifier-based method for categorizing slow waves as type I and type II based on ongoing EEG recordings is being developed.

Anatomical structures underlying Synchronization Process I most likely include arousal-promoting neuromodulatory systems with diffuse thalamic and/or cortical projections, but also matrix cells in the thalamus, which have diffuse cortical projections as well, especially to layer I.[64] The hypothesis that these diffusely projecting subcortical structures are functionally and anatomically related to the majority of slow waves occurring early in the falling-asleep period is supported by several lines of evidence. As described previously, the preferential region of origin of these slow waves contains the highest degree of noradrenergic innervation in the human and monkey cortex,[57-59] suggesting a tight link to the arousal-promoting noradrenergic system. Projections to the cortex that target preferentially the frontal medial area (corresponding to the region of primary involvement of most slow waves occurring early in the falling-asleep period) have also been described for the pontine and mesencephalic reticular formation [65], another arousal-promoting structure. In the rodent, the ventromedial thalamic nucleus, containing a high proportion of matrix cells with diffuse cortical projections, especially to layer I,[66] heavily innervates the sensorimotor[67,68] and anterior cingulate cortices,[67] consistent with the preferential origins and frontal medial involvement of slow waves occurring early in the falling- asleep period. In addition, a recent study has demonstrated that network states in the primary motor cortex are rapidly and strongly modulated by neurons in the primary somatosensory cortex,[69] suggesting that a rapid spread of slow waves across these two regions is possible. The common input to widespread regions of the cortex from a diffusely projecting subcortical source should lead to the near-simultaneous depolarization of many neurons widely distributed over the cortex, resulting in a particularly fast and efficient slow wave synchronization. Hence, a "bottom-up" synchronization would lead to slow waves that are large, have a steep slope, few negative peaks, and involve broad cortical regions, which are the characteristics associated with most slow waves occurring early in the falling-asleep period. Studies using intracellular recordings[70,71] have shown that gamma activity, reflecting a high firing rate of cortical neurons, is suppressed close to the negative peak of the slow wave (corresponding to the down state) and increases after the peak (during the phase corresponding to the upstate). Thus, a strong neural synchronization would result in an intense and brief decrease in gamma power tightly coupled with the positive to negative deflection of the slow wave (corresponding to the down state of cortical neurons; Figure S4), again consistent with findings in slow waves in the early part of the falling-asleep period.

In contrast, type II slow waves would occur when a slow oscillation is initiated in a local region of the cortex, most likely in layer V cells,[72] which then progressively recruit other neurons through a synchronization process mediated primarily by "horizontal," corticocortical connections (Synchronization Process II). This type of synchronization is presumably less efficient, as each local group of neurons can only depolarize directly connected neurons, to a degree that depends on the strength and extent of cortical connections in a particular region. This should result in slow waves that originate independently in many regions of the cortex, have a smaller amplitude, a flatter slope, more negative peaks, involve more circumscribed parts of the cortex, and are associated with a less sharp and pronounced decrease in gamma power during the down state (Figure 7). These characteristics were associated with the majority of slow waves occurring late in the falling-asleep period.

Relation of Type I Slow Waves to K-Complexes

K-complexes, as they are typically described in the literature, share several features with type I slow waves: they represent the first slow waves to occur in the NREM sleep cycle, tend to be isolated,[73] have a large amplitude[74] and a long duration,[74] and reach an amplitude maximum over frontal brain regions.[75,76] In addition, the fact that K-complexes can be elicited by sensory stimuli,[77-81] are associated with signs of autonomic activation,[82-86] and are sometimes followed by an EEG arousal[87] suggests that they may be functionally related to arousal systems. It thus appears that at least some type I slow waves represent what is traditionally called a K-complex, whereas type II slow waves often correspond to "delta" waves.[88] Nevertheless, the distinction between type I and type II slow waves appears to be preferable to the traditional distinction between "K-complexes" and "delta waves." First, the separation between "K-complexes" and

"delta waves" is potentially misleading, as it seems to imply that the two EEG graphoelements represent fundamentally different phenomena, where instead they are both slow waves, because of the same mechanism of membrane potential bistability in cortical cells.[89] Second, "K-complexes" and "delta waves" are loosely defined, based mainly on their visual morphology in the EEG. Instead, the distinction between type I and type II slow waves results from the unbiased categorization of two naturally dissociated and intersecting processes during the transition to sleep. Third, the proposed separation between type I and type II slow waves takes into account several additional parameters, such as slope, origin, and the topography of cortical involvement of slow waves. Finally, based on their various characteristics, it can be proposed that type I and type II slow waves, while reflecting the same cellular phenomenon of bistability, nevertheless result from different synchronization processes, the former through subcortical common input and the latter through intracortical spread.

Spindles in the Falling-Asleep Period

Our results demonstrate that sleep spindles also undergo a number of important changes during the falling-asleep period. Whereas early in the wake-sleep transition spindles are relatively sparse, predominantly local and have a high frequency, they become progressively more numerous, diffuse, and slower.

The fact that spindle density increased in the first part of the falling-asleep period, reached a maximum and then decreased, is in agreement with previous studies based on power spectrum analyses.[90,91] This course mirrors the evolution of slow wave density, as previously described.[90] Our results also confirm that spindle frequency decreases and that their duration increases in the course of the falling-asleep period,[4,92] consistent with a progressive hyperpolarization of thalamocortical cells.[93-94] In line with these findings and with previous studies,[39] we found that spindles preceding the negative peak of the slow wave (progressive hyperpolarization) were slower than spindles occurring after the slow wave peak (transition to a depolarized up state) (Figure S9). By evaluating the simultaneous occurrence of spindles across all scalp derivations, we demonstrated that after an initial prevalence of local spindles, the proportion of diffuse spindles increased progressively during the falling-asleep period. It should be noted that although spindles became more diffuse, overall, their cortical involvement remained limited, generally to less than 50% of channels. This is in line with studies using intracerebral EEG recordings showing that spindles tend to appear asynchronously across different brain regions.[3,4] In agreement with previous work, the extent of scalp involvement strongly correlated with spindle amplitude[3,4] and to a lesser extent with spindle duration. The degree of scalp involvement observed in the second part of the FAS is comparable to that obtained by intracranial recordings in established N2-stage sleep.[4] It has been proposed that spindle synchronization may depend on the interaction between a focally projecting "core" and a diffusely projecting "matrix" thalamic system that is mediated at the cortical level.[64,94,95] The transition from predominantly local to diffuse, synchronized spindles suggests that the falling-asleep period is characterized by dynamic changes in the degree of interaction between core and matrix systems.

Finally, source localization analyses confirmed previously described origins for frontal and centroparietal spindles in the medial/lateral prefrontal cortex and the precuneus, respectively.[37] In line with the transition from strictly focal to more diffuse spindles, the current results revealed that centroparietal spindles appearing in the initial phases of the falling-asleep period tend to remain more "local," whereas later spindles have a greater probability to involve more anterior brain areas. In parallel, for frontal spindles, the relative proportion of posteromedial parietal origins increased toward the end of the falling-asleep period. Conversely, no changes in parietal involvement were detected for spindles originating in frontal areas, although a relative increase in origin probability within prefrontal cortex was observed for late parietal spindles. These findings are in line with previous studies demonstrating that high-frequency centroparietal spindles commonly precede the appearance of lower frequency spindles in more anterior brain areas,[3,4,94] but also suggest that the opposite dynamic (that is, the involvement of posterior regions from spindles originating in frontal areas) is possible, although less likely. In addition, a recent study demonstrated that frontal spindles preferentially propagate in a posterior to anterior direction.[96] One proposed explanation for this phenomenon is that spindles propagate along the reticular nucleus, gradually recruiting different nuclei projecting to the cortex.[4] Taken together, the parallel increase in the degree of spindle synchronization and of frontal involvement of parietal spindles could reflect the existence of a common underlying mechanism or common changes in thalamocortical interactions.

Overall, we observed characteristic regional changes in spindle features in the falling-asleep period, in agreement with recent results indicating a local regulation of sleep spindles.[3,4] These findings add supporting evidence for the existence of independent spindle generators,[97,98] which display specific regional distributions and temporal characteristics in the course of the falling-asleep period.

Limitations of the Study

Although the study paradigm and imaging modality (hd-EEG) used in this study are particularly well suited for the purpose of studying spindles and slow waves in the transition to sleep, several caveats need to be discussed. First, there remains the fundamental limitation that infinitely many cortical current distributions can give rise to a given scalp voltage topography.[99] Source-modeling therefore remains, despite recent improvements, an approximate approach. Moreover, the falling-asleep epochs considered for analysis represent select episodes, free of artifacts and major arousals, and may therefore not be fully representative of physiological wake-sleep transitions. However, this selection enabled us to keep recording segments as a whole, without discarding any parts. This was important in order to guarantee the temporal continuity of the recordings, which in turn allowed us to compare falling-asleep periods of different lengths. Also, the fact that the results of our power analysis are in line previous studies[13,14,16,18,100] suggests that our findings can be generalized beyond our sample. It should also be noted that the data segments were acquired at different times of the night, which most likely resulted in variable sleep pressures that may have differentially affected the falling-asleep process. Future studies should systematically assess how sleep pressure

affects the transition to sleep. Further, we based our analysis on the assumption that the falling-asleep period is a process, evolving from the EA to the FSS regardless of the "absolute" time it takes to do so, and one may question whether this assumption is valid. On the other hand, there is *a priori* no good reason to assume that the regional distribution of spindles and slow waves should be fundamentally different in short and long falling-asleep segments. In addition, this is a commonly used procedure in sleep studies,[18,30,31] which offers the distinct advantage that it can be applied to falling-asleep periods of different durations. Finally, although our data are suggestive of a distinction between a subcorticocortical and a corticocortical synchronization mechanism underlying type I and type II slow waves, respectively, they cannot demonstrate directly or conclusively that these two mechanisms can be dissociated experimentally and lead to different types of slow waves. Future studies should be able to address this issue, for example by comparing peripheral stimulation with direct cortical stimulation.

Conclusions

Our findings show that the falling-asleep process is regionally heterogeneous. With respect to slow waves, we observed two spatially and temporally dissociated processes. At the beginning of the falling asleep period, isolated, large-amplitude slow waves prevailed. They involved broad areas of the cortex, predominated over frontomedial regions and preferentially originated from the sensorimotor and the posteromedial parietal cortex. Towards the end of the falling asleep period, slow waves were more numerous and had a smaller amplitude. They involved fewer cortical areas and had more evenly distributed origins. Spindles were initially sparse, fast and involved few cortical regions, then became more numerous and slower, and involved more areas.

Based on these results, we hypothesize the existence of two synchronization processes: (1) a "bottom-up," subcorticocortical, arousal system-dependent process that predominates in the early phase and leads to type I slow waves, and (2) a "horizontal," corticocortical synchronization process that predominates in the late phase and leads to type II slow waves.

Future Directions

The fact that in the early phase of the falling-asleep period, slow waves typically involve some regions (the frontal cortex, particularly the medial region) more than others (the occipital, temporal, and lateral posterior parietal areas) may relate to mental activity: perhaps it explains why sleep onset experiences are highly visual and frequently characterized by vestibular sensations[101] (considering that the primary visual cortex and the lateral parietotemporal areas are less affected by slow waves, and thus "more awake") and why the dreamer generally lacks insight into the hallucinatory character of the experience as compared to wakefulness[102,103] (given that the prefrontal regions are more involved by slow waves and thus "more asleep"). In line with this suggestion, recent studies have demonstrated specific occipital activity[18] in relation with hypnagogic imagery.[104] Future studies will investigate how regional changes in slow waves and spindles in the transition to sleep relate to the phenomenology of mental activity. To elucidate the functional role of the two synchronization processes, one could systematically investigate how they are modulated by sleep pressure and neural plasticity, as these factors have been shown to specifically affect the cortical distribution[7] as well as the slope and amplitude[32] of slow waves. It would also be of interest to determine if the temporal sequence that we observed in the falling- asleep period, with arousal-related cortical areas "falling asleep" before other cortical regions, is similar upon awakening. A positron emission tomography study[105] suggests that this is indeed so: after awakening from NREM sleep, cerebral blood flow was most rapidly reestablished in centrencephalic regions (brainstem, thalamus), indicating that these were the areas that "woke up" first, while in heteromodal neocortical areas, blood flow continued to increase until 20 min later, implying that these areas "woke up" last. A similar dissociation between centrencephalic and lateral cortical regions has been observed in a case of sleepwalking, a form of pathological awakening.[9] Finally, one could investigate how the two slow wave synchronization processes outlined here relate to wake-sleep transitions in sleep disorders such as insomnias, hypersomnias, and parasomnias, with potential diagnostic and therapeutic implications.

ACKNOWLEDGMENTS

Dr. Siclari and Dr. Bernardi contributed equally to this work.

DISCLOSURE STATEMENT

This was not an industry supported study. This work was supported by the Swiss National Science Foundation and the Swiss Foundation for Medical-Biological Grants (Grants 139778 and 145763, to Dr. Francesca Siclari), the Wisconsin Rath Distinguished Graduate Fellowship (to Mr. LaRocque), and the NIH (R01MH099231, to Dr. Tononi). Dr. Tononi is a consultant to Philips Healthcare who endowed the David P. White Chair in Sleep Medicine, held by Dr. Tononi at the University of Wisconsin-Madison. Philips Healthcare also sponsors a grant on Slow Wave Induction. Dr. Tononi was a symposium speaker for Philips Healthcare, and also spoke at a symposium on Slow Wave Sleep for Sanofi. Dr. Riedner receives partial salary support from the Philips Healthcare Grant held by Dr. Tononi. Dr. Benca has served as a consultant for Merck and Orexigen Therapeutics, Inc. and receives grant support from Merck. The other authors have indicated no financial conflicts of interest.

REFERENCES

1. Jones BE. From waking to sleeping: neuronal and chemical substrates. Trends Pharmacol Sci 2005;26:578-86.
2. Steriade M. Corticothalamic resonance, states of vigilance and mentation. Neuroscience 2000;101:243-76.
3. Nir Y, Staba RJ, Andrillon T, et al. Regional slow waves and spindles in human sleep. Neuron 2011;70:153-69.
4. Andrillon T, Nir Y, Staba RJ, et al. Sleep spindles in humans: insights from intracranial EEG and unit recordings. J Neurosci 2011;31:17821-34.
5. Esser SK, Huber R, Massimini M, Peterson MJ, Ferrarelli F, Tononi G. A direct demonstration of cortical LTP in humans: a combined TMS/EEG study. Brain Res Bull 2006;69:86-94.
6. Huber R, Ghilardi MF, Massimini M, et al. Arm immobilization causes cortical plastic changes and locally decreases sleep slow wave activity. Nat Neurosci 2006;9:1169-76.
7. Huber R, Ghilardi MF, Massimini M, Tononi G. Local sleep and learning. Nature 2004;430:78-81.
8. Hung CS, Sarasso S, Ferrarelli F, et al. Local experience-dependent changes in the wake EEG after prolonged wakefulness. Sleep 2013;36:59-72.

9. Bassetti C, Vella S, Donati F, Wielepp P, Weder B. SPECT during sleepwalking. Lancet 2000;356:484-5.
10. Terzaghi M, Sartori I, Tassi L, et al. Evidence of dissociated arousal states during NREM parasomnia from an intracerebral neurophysiological study. Sleep 2009;32:409-12.
11. Mahowald MW. What state dissociation can teach us about consciousness and the function of sleep. Sleep Med 2008;10:159-60.
12. Zadra A, Desautels A, Petit D, Montplaisir J. Somnambulism: clinical aspects and pathophysiological hypotheses. Lancet Neurol 2013;12:285-94.
13. De Gennaro L, Ferrara M, Curcio G, Cristiani R. Antero-posterior EEG changes during the wakefulness-sleep transition. Clin Neurophysiol 2001;112:1901-11.
14. Tanaka H, Hayashi M, Hori T. Topographical characteristics of slow wave activities during the transition from wakefulness to sleep. Clin Neurophysiol 2000;111:417-27.
15. Wright KP, Jr., Badia P, Wauquier A. Topographical and temporal patterns of brain activity during the transition from wakefulness to sleep. Sleep 1995;18:880-9.
16. Hori T. Spatiotemporal changes of EEG activity during waking-sleeping transition period. Int J Neurosci 1985;27:101-14.
17. Hasan J, Broughton RC. Quantitative topographic EEG mapping during drowsiness and sleep onset. In: Ogilvie RD, Harsh JR, eds. Sleep Onset: Normal and Abnormal Processes. Washington: American Psychological Association, 1994.
18. Marzano C, Moroni F, Gorgoni M, Nobili L, Ferrara M, De Gennaro L. How we fall asleep: regional and temporal differences in electroencephalographic synchronization at sleep onset. Sleep Med 2013;14:1112-22.
19. Casagrande M, Bertini M. Laterality of the sleep onset process: which hemisphere goes to sleep first? Biol Psychol 2008;77:76-80.
20. Magnin M, Rey M, Bastuji H, Guillemant P, Mauguiere F, Garcia-Larrea L. Thalamic deactivation at sleep onset precedes that of the cerebral cortex in humans. Proc Natl Acad Sci U S A 2010;107:3829-33.
21. Poudel GR, Innes CR, Bones PJ, Watts R, Jones RD. Losing the struggle to stay awake: divergent thalamic and cortical activity during microsleeps. Hum Brain Mapp 2014;35:257-69.
22. Kaufmann C, Wehrle R, Wetter TC, et al. Brain activation and hypothalamic functional connectivity during human non-rapid eye movement sleep: an EEG/fMRI study. Brain 2006;129:655-67.
23. Samann PG, Wehrle R, Hoehn D, et al. Development of the brain's default mode network from wakefulness to slow wave sleep. Cereb Cortex 2011;21:2082-93.
24. Sarasso S, Proserpio P, Pigorini A, et al. Hippocampal sleep spindles preceding neocortical sleep onset in humans. Neuroimage 2014;86:425-32.
25. Siclari F, Larocque JJ, Postle BR, Tononi G. Assessing sleep consciousness within subjects using a serial awakening paradigm. Front Psychol 2013;4:542.
26. Iber C, Ancoli-Israel S, Chesson A, Quan SF. The AASM Manual for the Scoring of Sleep and Associated Events: Rules, Terminology and Technical Specifications. 1st ed. Westchester, Illinois: American Academy of Sleep Medicine, 2007.
27. Ogilvie RD. The process of falling asleep. Sleep Med Rev 2001;5:247-70.
28. Delorme A, Makeig S. EEGLAB: an open source toolbox for analysis of single-trial EEG dynamics including independent component analysis. J Neurosci Methods 2004;134:9-21.
29. Jung TP, Makeig S, Humphries C, et al. Removing electroencephalographic artifacts by blind source separation. Psychophysiology 2000;37:163-78.
30. Putilov AA, Donskaya OG. Rapid changes in scores on the two largest principal components of the electroencephalographic spectrum demarcate the boundaries of drowsy sleep. Sleep Biol Rhythms 2013;11:154-64.
31. Aeschbach D, Borbely AA. All-night dynamics of the human sleep EEG. J Sleep Res 1993;2:70-81.
32. Riedner BA, Vyazovskiy VV, Huber R, et al. Sleep homeostasis and cortical synchronization: III. A high-density EEG study of sleep slow waves in humans. Sleep 2007;30:1643-57.
33. Pascual-Marqui RD. Standardized low-resolution brain electromagnetic tomography (sLORETA): technical details. Methods Find Exp Clin Pharmacol 2002;24 Suppl D:5-12.
34. Murphy M, Riedner BA, Huber R, Massimini M, Ferrarelli F, Tononi G. Source modeling sleep slow waves. Proc Natl Acad Sci U S A 2009;106:1608-13.
35. Valderrama M, Crepon B, Botella-Soler V, et al. Human gamma oscillations during slow wave sleep. PLoS One 2012;7:e33477.
36. Ferrarelli F, Huber R, Peterson MJ, et al. Reduced sleep spindle activity in schizophrenia patients. Am J Psychiatry 2007;164:483-92.
37. Anderer P, Klosch G, Gruber G, et al. Low-resolution brain electromagnetic tomography revealed simultaneously active frontal and parietal sleep spindle sources in the human cortex. Neuroscience 2001;103:581-92.
38. De Gennaro L, Ferrara M. Sleep spindles: an overview. Sleep Med Rev 2003;7:423-40.
39. Molle M, Bergmann TO, Marshall L, Born J. Fast and slow spindles during the sleep slow oscillation: disparate coalescence and engagement in memory processing. Sleep 2011;34:1411-21.
40. Steriade M, Contreras D, Amzica F, Timofeev I. Synchronization of fast (30-40 Hz) spontaneous oscillations in intrathalamic and thalamocortical networks. J Neurosci 1996;16:2788-808.
41. Bastien CH, Crowley KE, Colrain IM. Evoked potential components unique to non-REM sleep: relationship to evoked K-complexes and vertex sharp waves. Int J Psychophysiol 2002;46:257-74.
42. Werth E, Achermann P, Dijk DJ, Borbely AA. Spindle frequency activity in the sleep EEG: individual differences and topographic distribution. Electroencephalogr Clin Neurophysiol 1997;103:535-42.
43. Jankel WR, Niedermeyer E. Sleep spindles. J Clin Neurophysiol 1985;2:1-35.
44. Sarasso S, Proserpio P, Pigorini A, et al. Hippocampal sleep spindles preceding neocortical sleep onset in humans. Neuroimage 2014;86:425-32.
45. Kandel A, Buzsaki G. Cellular-synaptic generation of sleep spindles, spike-and-wave discharges, and evoked thalamocortical responses in the neocortex of the rat. J Neurosci 1997;17:6783-97.
46. Steriade M. Grouping of brain rhythms in corticothalamic systems. Neuroscience 2006;137:1087-106.
47. Steriade M, Timofeev I, Grenier F. Natural waking and sleep states: a view from inside neocortical neurons. J Neurophysiol 2001;85:1969-85.
48. Steriade M, Amzica F, Nunez A. Cholinergic and noradrenergic modulation of the slow (approximately 0.3 Hz) oscillation in neocortical cells. J Neurophysiol 1993;70:1385-400.
49. Steriade M, Nunez A, Amzica F. A novel slow (< 1 Hz) oscillation of neocortical neurons in vivo: depolarizing and hyperpolarizing components. J Neurosci 1993;13:3252-65.
50. Amzica F, Steriade M. Electrophysiological correlates of sleep delta waves. Electroencephalogr Clin Neurophysiol 1998;107:69-83.
51. Vyazovskiy VV, Olcese U, Lazimy YM, et al. Cortical firing and sleep homeostasis. Neuron 2009;63:865-78.
52. Crunelli V, Hughes SW. The slow (< 1 Hz) rhythm of non-REM sleep: a dialogue between three cardinal oscillators. Nat Neurosci 2010;13:9-17.
53. Timofeev I, Grenier F, Bazhenov M, Sejnowski TJ, Steriade M. Origin of slow cortical oscillations in deafferented cortical slabs. Cereb Cortex 2000;10:1185-99.
54. Shu Y, Hasenstaub A, McCormick DA. Turning on and off recurrent balanced cortical activity. Nature 2003;423:288-93.
55. Dang-Vu TT, Schabus M, Desseilles M, et al. Spontaneous neural activity during human slow wave sleep. Proc Natl Acad Sci U S A 2008;105:15160-5.
56. Massimini M, Ferrarelli F, Esser SK, et al. Triggering sleep slow waves by transcranial magnetic stimulation. Proc Natl Acad Sci U S A 2007;104:8496-501.
57. Javoy-Agid F, Scatton B, Ruberg M, et al. Distribution of monoaminergic, cholinergic, and GABAergic markers in the human cerebral cortex. Neuroscience 1989;29:251-9.
58. Gaspar P, Berger B, Febvret A, Vigny A, Henry JP. Catecholamine innervation of the human cerebral cortex as revealed by comparative immunohistochemistry of tyrosine hydroxylase and dopamine-beta-hydroxylase. J Comp Neurol 1989;279:249-71.
59. Lewis DA, Morrison JH. Noradrenergic innervation of monkey prefrontal cortex: a dopamine-beta-hydroxylase immunohistochemical study. J Comp Neurol 1989;282:317-30.
60. Eschenko O, Magri C, Panzeri S, Sara SJ. Noradrenergic neurons of the locus coeruleus are phase locked to cortical up-down states during sleep. Cereb Cortex 2012;22:426-35.
61. Vyazovskiy VV, Faraguna U, Cirelli C, Tononi G. Triggering slow waves during NREM sleep in the rat by intracortical electrical stimulation: effects of sleep/wake history and background activity. J Neurophysiol 2009;101:1921-31.

62. Esser SK, Hill SL, Tononi G. Sleep homeostasis and cortical synchronization: I. Modeling the effects of synaptic strength on sleep slow waves. Sleep 2007;30:1617-30.
63. Vyazovskiy VV, Riedner BA, Cirelli C, Tononi G. Sleep homeostasis and cortical synchronization: II. A local field potential study of sleep slow waves in the rat. Sleep 2007;30:1631-42.
64. Jones EG. The thalamic matrix and thalamocortical synchrony. Trends Neurosci 2001;24:595-601.
65. Jones BE, Yang TZ. The efferent projections from the reticular formation and the locus coeruleus studied by anterograde and retrograde axonal transport in the rat. J Comp Neurol 1985;242:56-92.
66. Clasca F, Rubio-Garrido P, Jabaudon D. Unveiling the diversity of thalamocortical neuron subtypes. Eur J Neurosci 2012;35:1524-32.
67. Kuramoto E, Ohno S, Furuta T, et al. Ventral medial nucleus neurons send thalamocortical afferents more widely and more preferentially to layer 1 than neurons of the ventral anterior-ventral lateral nuclear complex in the rat. Cereb Cortex 2013 Aug 22. [Epub ahead of print]. http://dx.doi.org/10.1093/cercor/bht216.
68. Desbois C, Villanueva L. The organization of lateral ventromedial thalamic connections in the rat: a link for the distribution of nociceptive signals to widespread cortical regions. Neuroscience 2001;102:885-98.
69. Zagha E, Casale AE, Sachdev RN, McGinley MJ, McCormick DA. Motor cortex feedback influences sensory processing by modulating network state. Neuron 2013;79:567-78.
70. Steriade M, Amzica F, Contreras D. Synchronization of fast (30-40 Hz) spontaneous cortical rhythms during brain activation. J Neurosci 1996;16:392-417.
71. Mukovski M, Chauvette S, Timofeev I, Volgushev M. Detection of active and silent states in neocortical neurons from the field potential signal during slow-wave sleep. Cereb Cortex 2007;17:400-14.
72. Beltramo R, D'Urso G, Dal Maschio M, et al. Layer-specific excitatory circuits differentially control recurrent network dynamics in the neocortex. Nat Neurosci 2013;16:227-34.
73. Halasz P. K-complex, a reactive EEG graphoelement of NREM sleep: an old chap in a new garment. Sleep Med Rev 2005;9:391-412.
74. Bremer G, Smith JR, Karacan I. Automatic detection of the K-complex in sleep electroencephalograms. IEEE Trans Biomed Eng 1970;17:314-23.
75. Bastien C, Campbell K. The evoked K-complex: all-or-none phenomenon? Sleep 1992;15:236-45.
76. Wennberg R. Intracranial cortical localization of the human K-complex. Clin Neurophysiol 2010;121:1176-86.
77. Davis H, Davis PA, Loomis AL, Harvey E, Hobart G. Electrical reactions of human brain to auditory stimulation during sleep. J Neurophysiol 1939;2:500-14.
78. Roth M, Shaw J, Green J. The form voltage distribution and physiological significance of the K-complex. Electroencephalogr Clin Neurophysiol 1956;8:385-402.
79. Webster KE, Colrain IM. Multichannel EEG analysis of respiratory evoked-potential components during wakefulness and NREM sleep. J Appl Physiol 1998;85:1727-35.
80. Gora J, Colrain IM, Trinder J. The investigation of K-complex and vertex sharp wave activity in response to mid-inspiratory occlusions and complete obstructions to breathing during NREM sleep. Sleep 2001;24:81-9.
81. Riedner BA, Hulse BK, Murphy MJ, Ferrarelli F, Tononi G. Temporal dynamics of cortical sources underlying spontaneous and peripherally evoked slow waves. Prog Brain Res 2011;193:201-18.
82. Johnson L, Karpan WE. Autonomic correlates of the spontaneous K-complex. Psychophysiology 2007;4:444-53.
83. Pampiglione G, Ackner B. The effects of repeated stimuli upon EEG and vasomotor activity during sleep in man. Brain 1958;81:64-74.
84. Heald S, Siebers RW, Maling TJ. The k-complex vasoconstrictor response: evidence for central vasomotor downregulation in borderline hypertension. J Hypertens Suppl 1989;7:S28-9.
85. Hornyak M, Cejnar M, Elam M, Matousek M, Wallin BG. Sympathetic muscle nerve activity during sleep in man. Brain 1991;114 (Pt 3):1281-95.
86. Tank J, Diedrich A, Hale N, et al. Relationship between blood pressure, sleep K-complexes, and muscle sympathetic nerve activity in humans. Am J Physiol Regul Integr Comp Physiol 2003;285:R208-14.
87. Colrain IM. The K-complex: a 7-decade history. Sleep 2005;28:255-73.
88. Silber MH, Ancoli-Israel S, Bonnet MH, et al. The visual scoring of sleep in adults. J Clin Sleep Med 2007;3:121-31.
89. Cash SS, Halgren E, Dehghani N, et al. The human K-complex represents an isolated cortical down-state. Science 2009;324:1084-7.
90. Merica H, Fortune RD. State transitions between wake and sleep, and within the ultradian cycle, with focus on the link to neuronal activity. Sleep Med Rev 2004;8:473-85.
91. Uchida S, Atsumi Y, Kojima T. Dynamic relationships between sleep spindles and delta waves during a NREM period. Brain Res Bull 1994;33:351-5.
92. Himanen SL, Virkkala J, Huhtala H, Hasan J. Spindle frequencies in sleep EEG show U-shape within first four NREM sleep episodes. J Sleep Res 2002;11:35-42.
93. Hirsch JC, Fourment A, Marc ME. Sleep-related variations of membrane potential in the lateral geniculate body relay neurons of the cat. Brain Res 1983;259:308-12.
94. Dehghani N, Cash SS, Halgren E. Emergence of synchronous EEG spindles from asynchronous MEG spindles. Hum Brain Mapp 2011;32:2217-27.
95. Bonjean M, Baker T, Bazhenov M, Cash S, Halgren E, Sejnowski T. Interactions between core and matrix thalamocortical projections in human sleep spindle synchronization. J Neurosci 2012;32:5250-63.
96. O'Reilly C, Nielsen T. Assessing EEG sleep spindle propagation. Part 2: experimental characterization. J Neurosci Methods 2014;221:215-27.
97. Dehghani N, Cash SS, Chen CC, et al. Divergent cortical generators of MEG and EEG during human sleep spindles suggested by distributed source modeling. PLoS One 2010;5:e11454.
98. Dehghani N, Cash SS, Rossetti AO, Chen CC, Halgren E. Magnetoencephalography demonstrates multiple asynchronous generators during human sleep spindles. J Neurophysiol 2010;104:179-88.
99. Nunez PL, Srinivasan R. Electric fields of the brain: the neurophysics of EEG. Oxford: Oxford Univ Press, 2006.
100. Morikawa T, Hayashi M, Hori T. Spatiotemporal variations of alpha and sigma band EEG in the waking-sleeping transition period. Percept Mot Skills 2002;95:131-54.
101. Nir Y, Tononi G. Dreaming and the brain: from phenomenology to neurophysiology. Trends Cogn Sci 2010;14:88-100.
102. Yang CM, Han HY, Yang MH, Su WC, Lane T. What subjective experiences determine the perception of falling asleep during sleep onset period? Conscious Cogn 2010;19:1084-92.
103. Foulkes D, Vogel G. Mental Activity at Sleep Onset. J Abnorm Psychol 1965;70:231-43.
104. Horikawa T, Tamaki M, Miyawaki Y, Kamitani Y. Neural decoding of visual imagery during sleep. Science 2013;340:639-42.
105. Balkin TJ, Braun AR, Wesensten NJ, et al. The process of awakening: a PET study of regional brain activity patterns mediating the re-establishment of alertness and consciousness. Brain 2002;125:2308-19.
106. Massimini M, Huber R, Ferrarelli F, Hill S, Tononi G. The sleep slow oscillation as a traveling wave. J Neurosci 2004;24:6862-70.

SUPPLEMENTAL MATERIAL

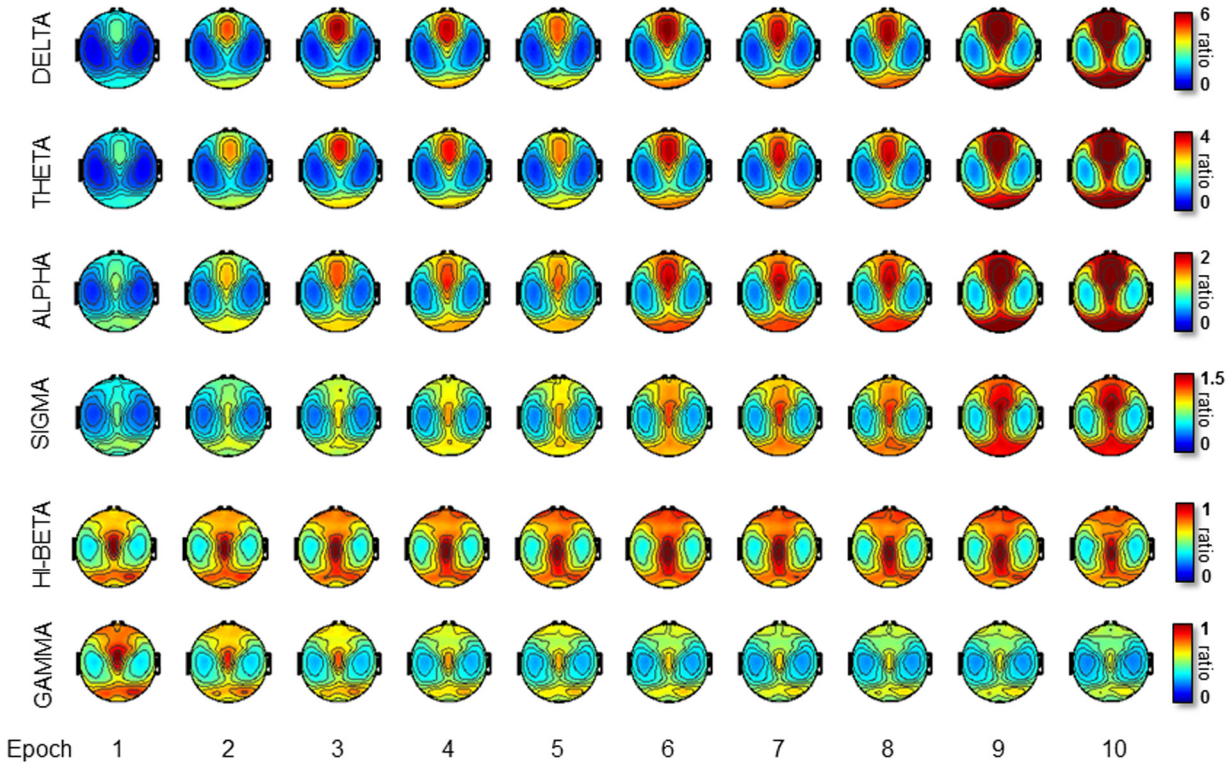

Figure S1—Power spectrum analysis: topographical electroencephalographic (EEG) changes. Topographical distribution of spectral power in different frequency bands (delta: 1.0–4.5 Hz, theta: 4.5–7.5 Hz, alpha: 8.0–12 Hz, sigma: 11–15 Hz, high beta: 20–25 Hz, low gamma: 25–40 Hz) for the 10 consecutive epochs of the falling asleep period (group average). Each falling asleep segment was divided in 10 epochs of equal duration, and the ratio with a presleep baseline (30 sec before the end of alpha activity) was computed. Then, for each subject, the average ratio between homologous epochs of different falling asleep segments was calculated for each channel.

Table S1—Characteristics of subjects and falling-asleep segments.

Subject	Sex	Age	FAS (n)	FAS length (min)
S1	M	28	33	9.4 ± 2.6
S2	F	31	19	8.2 ± 2.6
S3	F	21	25	10.9 ± 5.7
S4	F	25	27	7.8 ± 4.5
S5	M	27	19	8.6 ± 3.5
S6	M	38	18	4.6 ± 3.0
All	–	28.3 ± 5.8	23.5 ± 5.9	9.3 ± 2.1

FAS, falling-asleep segments.

Table S2—Characteristics of slow waves in early and late epochs for a single frontal channel computed at the group level (n = 6).

	Slow waves of early epochs	Slow waves of late epochs
Density (n/min)	5.4 ± 1.8 [a]	11.4 ± 3.0 [a]
Amplitude (μV)	120.16 ± 21.05 [a]	84.25 ± 14.48 [a]
Duration (s)	1.07 ± 0.13	0.96 ± 0.08
Slope 1 (μV/s)	1123.03 ± 151.60 [a]	922.38 ± 120.13 [a]
Slope 2 (μV/s)	1047.01 ± 130.22 [a]	810.16 ± 96.42 [a]
Negative peaks	1.80 ± 0.17	2.01 ± 0.07
Positive peaks	2.87 ± 0.51	2.47 ± 0.27

[a] Significant differences between slow waves in early and late epochs ($P < 0.05$).

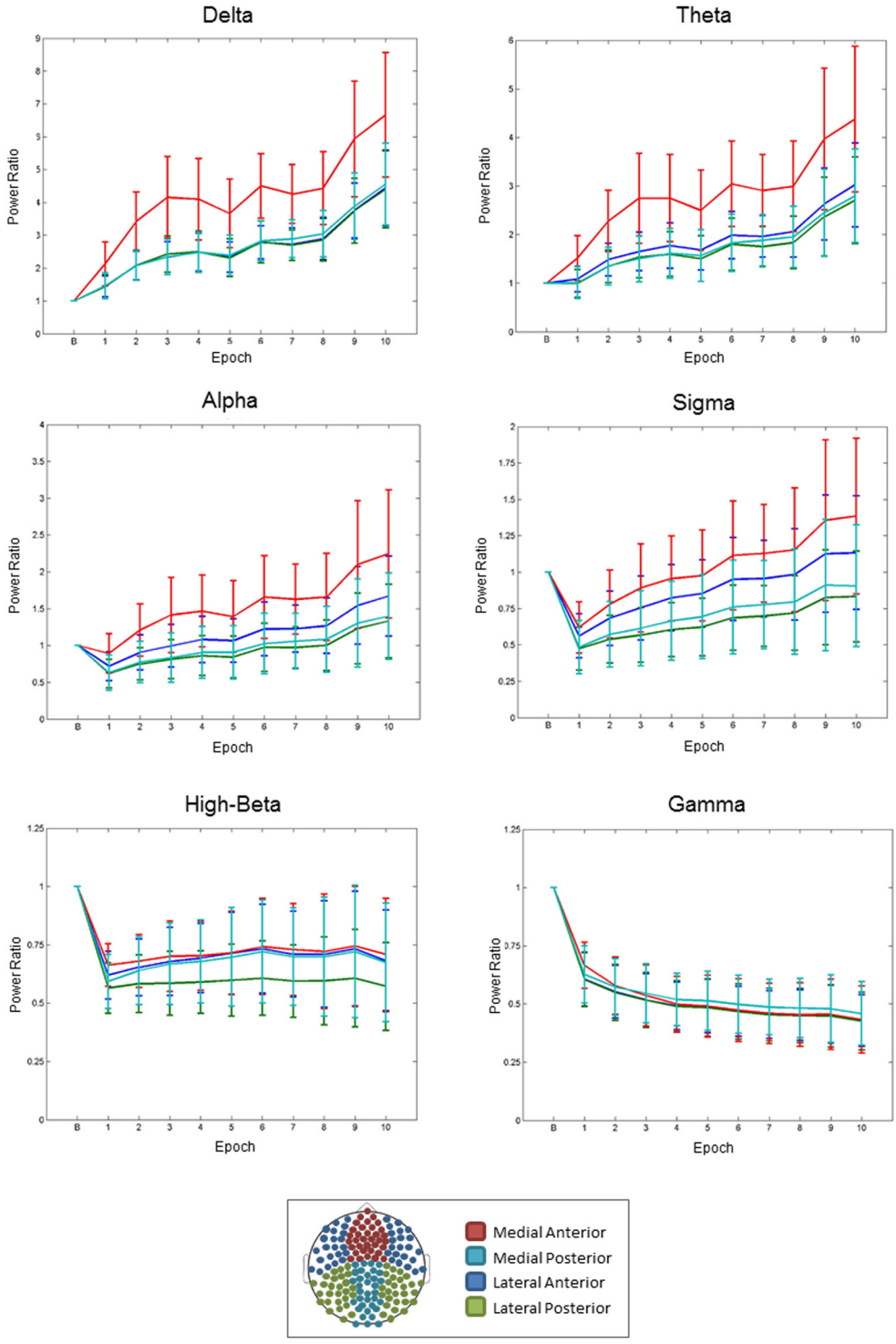

Figure S2—Power spectrum analysis: regional electroencephalographic (EEG) changes. Spectral power changes in different frequency bands (delta: 1.0–4.5 Hz, theta: 4.5–7.5 Hz, alpha: 8.0–12 Hz, sigma: 11–15 Hz, high beta: 20–25 Hz, low gamma: 25–40 Hz) for the four regions of interest (ROIs) and the 10 consecutive epochs of the falling asleep period (group average), including the presleep baseline (B). Each falling asleep period was divided in 10 epochs of equal duration, and the ratio with a presleep baseline (30 sec before the end of alpha activity) was computed. Then, for each subject, the average ratio between homologous epochs of different falling asleep processes was calculated for each channel.

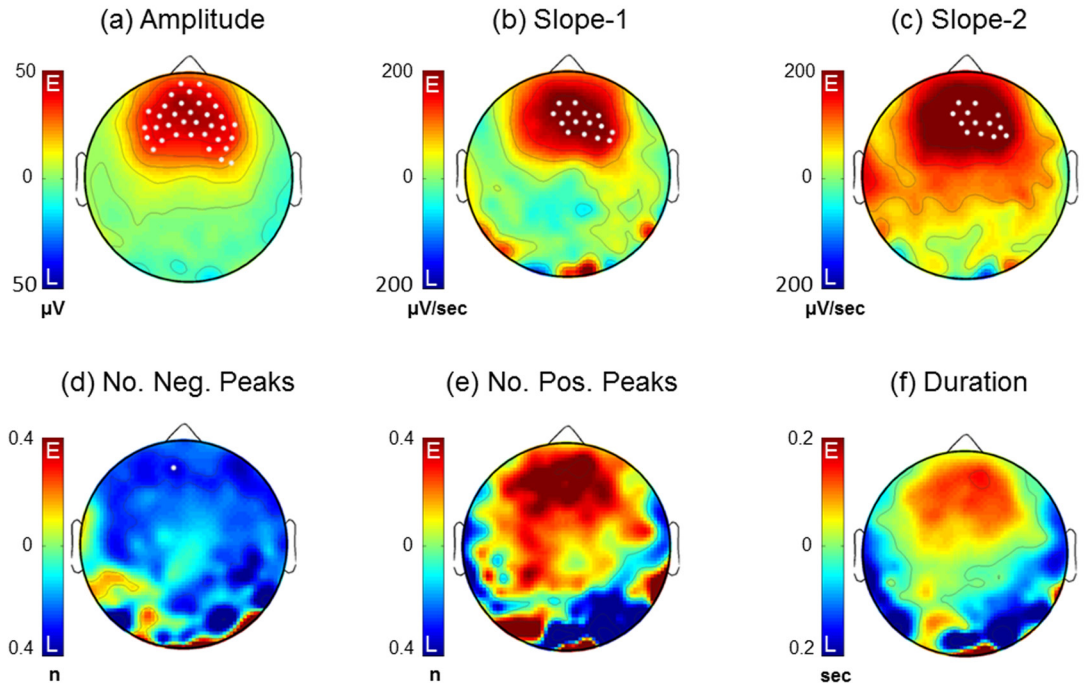

Figure S3—Differences between slow waves detected in early and late epochs. Topographical representation of the differences in slow wave amplitude (a), first slope (b), corresponding to the positive to negative deflection of the slow wave, second slope (c), corresponding to the negative to positive deflection of the slow wave, number of negative peaks per slow wave (d). number of positive peaks per slow wave (e), and duration (f) between slow waves detected in early (E) and late (L) epochs. Areas in which the parameter was higher in slow waves detected in early epochs appear red, areas in which it was higher in slow waves detected in late epochs appear blue. Dots indicate areas in which the differences were significant ($P < 0.05$) in at least five subjects.

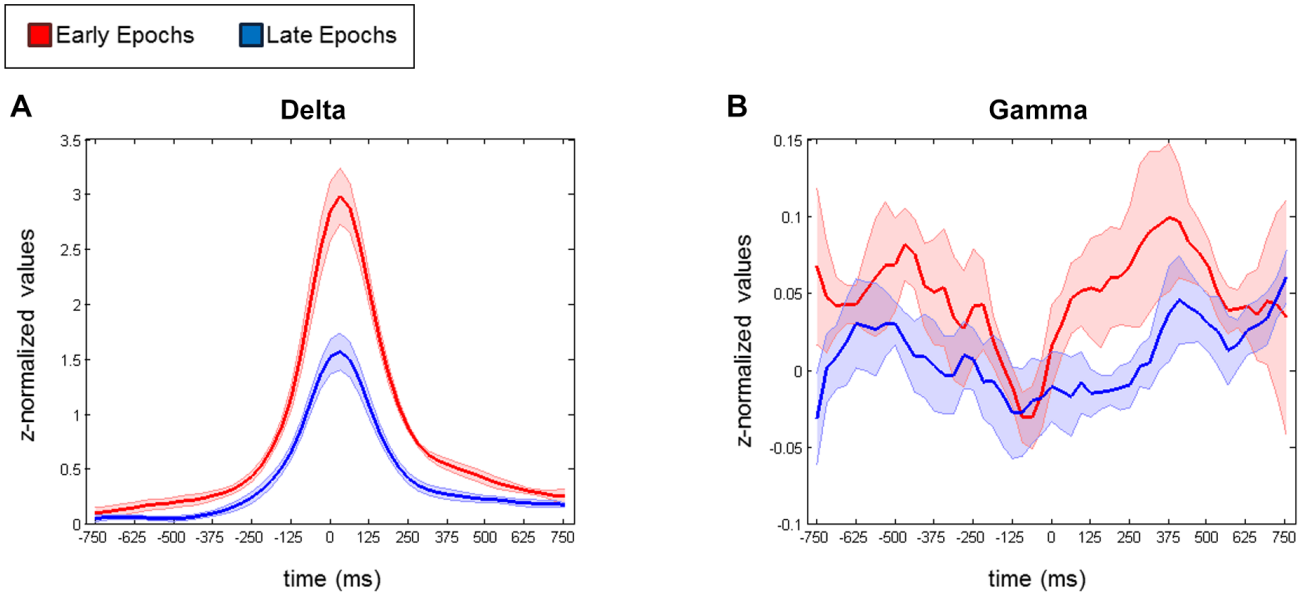

Figure S4—Delta and gamma power during slow waves detected in early and late epochs. Delta **(A)** and gamma **(B)** power centered around the negative peak of slow waves detected in early (red lines) and late (blue lines) epochs (± standard error, SE). For each slow wave detected in a single frontal channel (Fz), we computed the root mean square (RMS, 31.25 ms time-window) of the delta (0.5-4 Hz) and gamma (30–50 Hz) power in the 10 sec centered around the negative peak of the wave. For each subject delta and gamma RMS time series were z-score transformed and averaged across all the detected slow waves. A group average was computed on the 1.5 sec centered on the negative peak of the slow wave. Gamma power associated with slow waves detected in early epochs was characterized by a sharp decrease during the 250 ms preceding the negative peak, and by a rapid increase which started immediately after this point. In slow waves detected during late epochs this increase was slower and less pronounced. Specifically, gamma power within with the 250 ms following the slow wave negative peak was significantly different for slow waves detected in early and late epochs (signed rank test, $P < 0.05$). In this image a smoothing (five points moving average) was also applied to improve graphs readability.

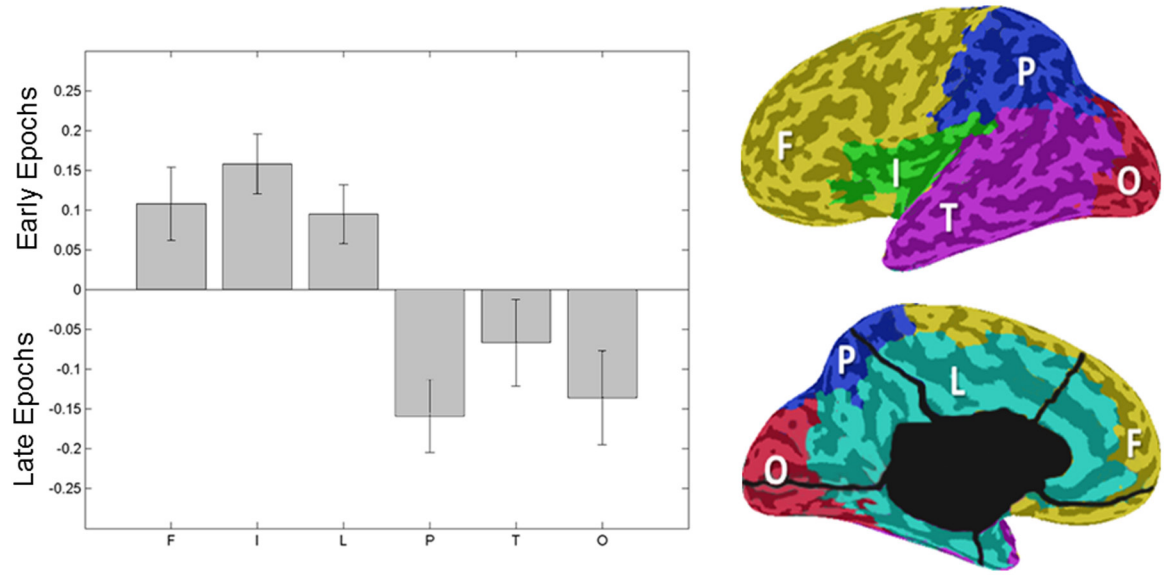

Figure S5—Regional differences in origin probability distribution between slow waves detected in early and late epochs. For the early and late epochs of the falling-asleep process, the probability of having a slow wave origin within each region of interest (ROI) defined in source space (inflated cortical maps with colors representing the different ROIs, are shown on the right) is compared with the mean probability observed across all ROIs. The origin of an individual slow wave in source space was defined as the top 10% voxels, which showed the earliest relative current maxima, identified within a time-window of 100 ms centered on the negative voltage peak of the slow wave (a threshold corresponding to 25% of the maximum relative current value was also applied). Slow waves detected in early epochs originated more frequently within frontal [F], insular [I] and limbic [L] areas, while slow waves detected in late epochs showed a relative increase in origin probability within more posterior brain regions, including parietal [P], temporal [T] and occipital [O] cortex.

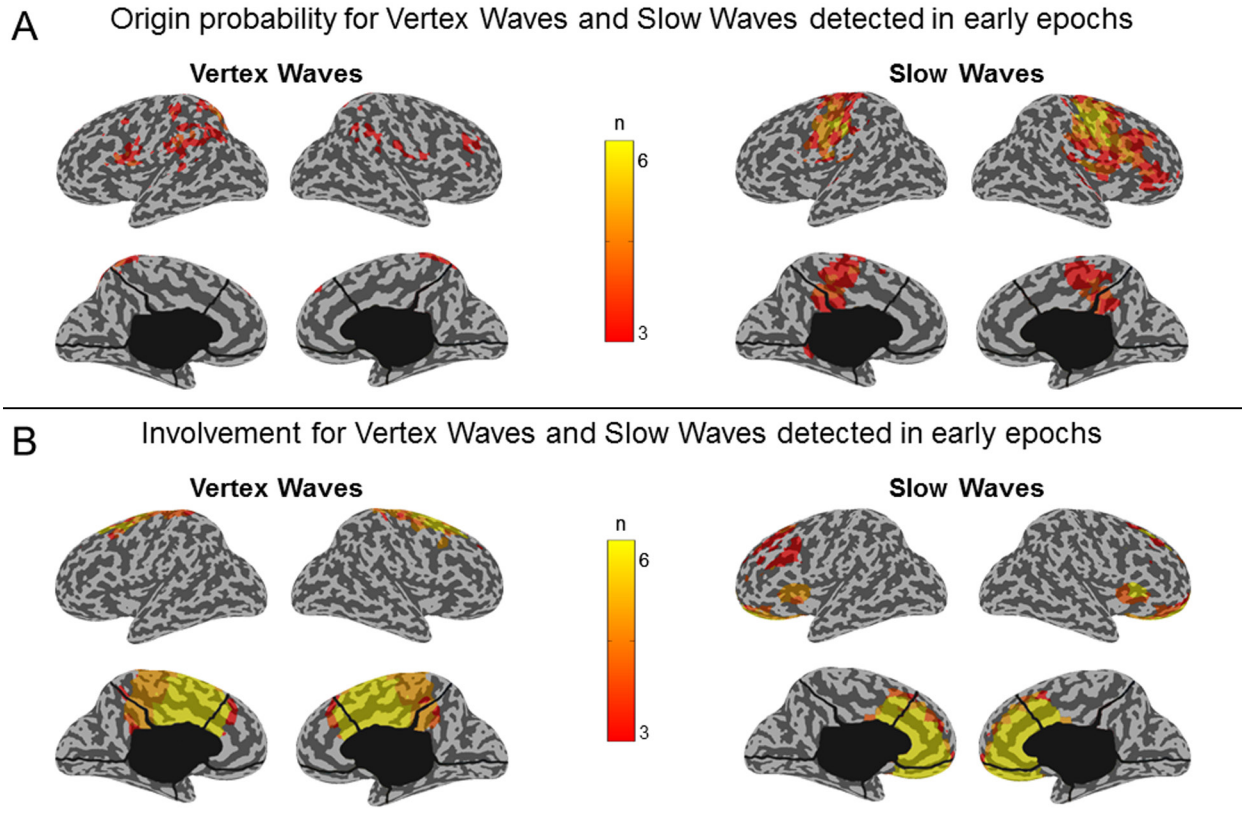

Figure S6—Origins and involvement of vertex waves and slow waves detected in early epochs. **(A)** Most frequent origins (top 10% in at least three of six subjects) for vertex waves and slow waves detected in early epochs. **(B)** Involvement (defined as the average of the relative current achieved within a time-window of 100 ms centered on the negative voltage peak of the slow wave) for vertex waves and slow waves. For this analysis vertex waves were defined as waves with a duration between 0.1 and 0.25 sec and a negative peak amplitude greater than 40 μV.

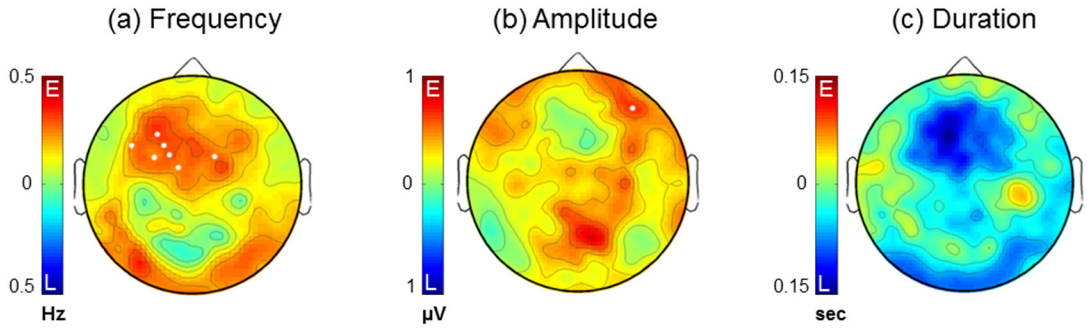

Figure S7—Differences between early and late spindles. Topographical representation of differences in spindle frequency (a), amplitude (b) and duration (c) between early (E) and late (L) spindles. Areas in which the parameter was higher in early spindles appear red; areas in which it was higher in late spindles appear blue. Dots indicate areas in which differences were significant ($P < 0.05$) in at least five subjects.

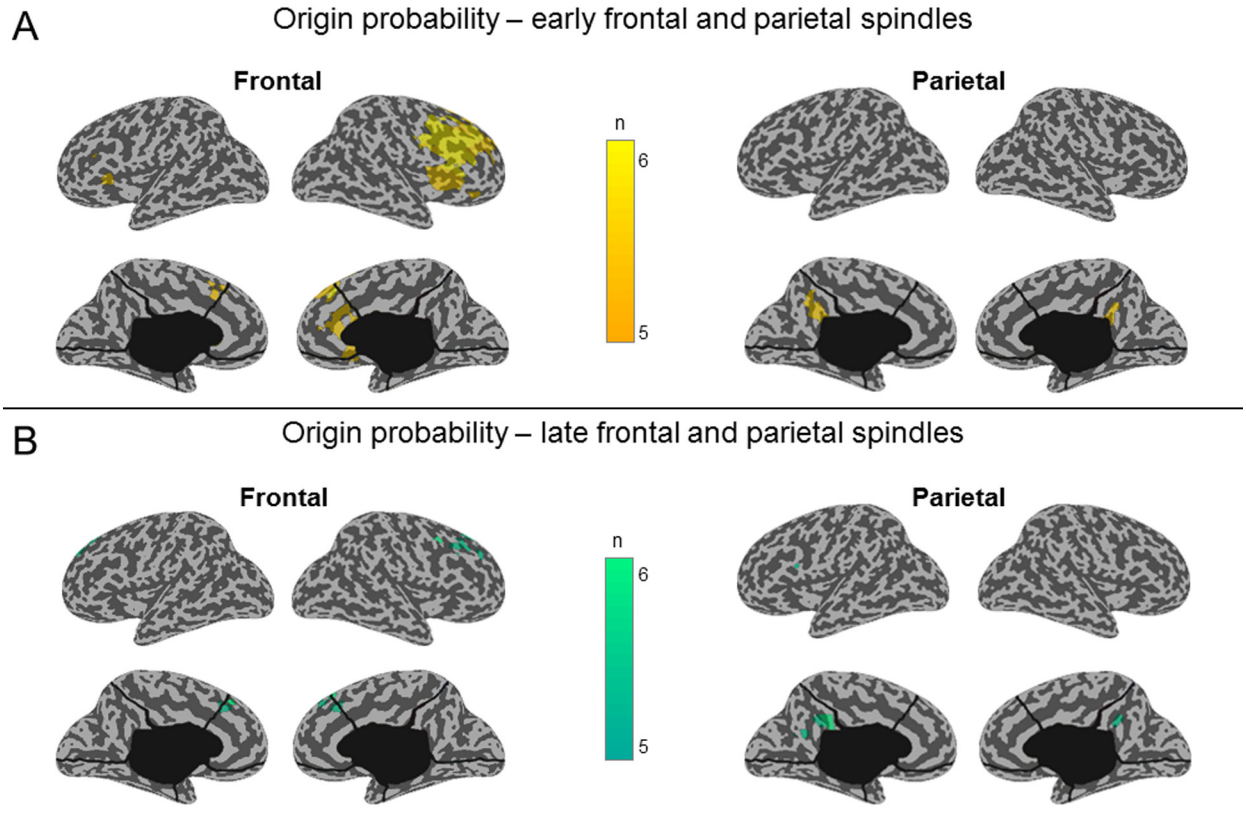

Figure S8—Origin probability for early and late spindles. Most frequent origins (top 10% in at least five of six subjects) for frontal **(A)** and centroparietal **(B)** spindles. We determined the probabilistic origin defined as the top 10% voxels, which showed the earliest relative current maxima after the beginning of the spindle. Only relative current maxima above a threshold of 50% of the absolute maximum identified across all dipoles were included in this analysis.

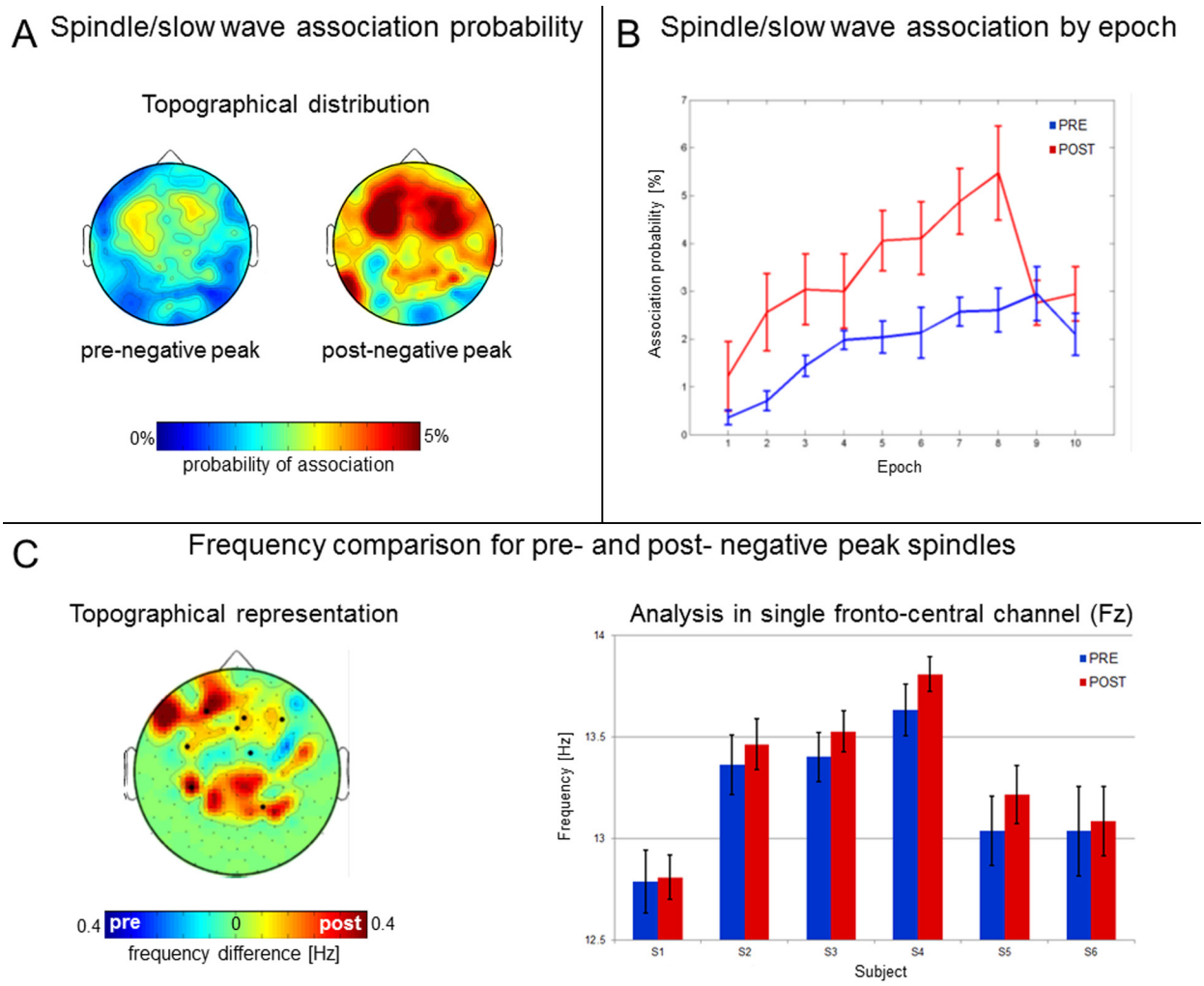

Figure S9—Association of slow waves and spindles. **(A)** Topographical distribution of the association probability (i.e., the probability for a slow wave to be associated with a spindle) for prepeak (left) and postpeak (right) spindles (group average). **(B)** Evolution of the association probability [%] over the 10 consecutive epochs of the falling asleep period (group average), for prepeak (blue) and postpeak (red) spindles. **(C)** Comparison of spindle frequency [Hz] for prepeak (blue) and postpeak (red) spindles (left). Black dots indicate significant differences at the 0.05 level. Only electrodes with at least one detected spindle in all subjects were included. **(C)** Comparison of spindle frequencies [Hz] between prepeak (blue) and postpeak (red) spindles in a frontocentral channel (Fz) at the single subject level (right).